Indian J Radio & Space Phys, Vol. 13, No. 1, pp. 1-34
FEBRUARY 1984
CODEN: IJRSAK ISSN: 0367-8393
13(1) 1-34 (1984)

INDIAN JOURNAL OF RADIO & SPACE PHYSICS

Indian Agricultural Statistics
276
Dy/Acs No
Dat 2/7/84
Old Road LUDHIANA

Published by
PUBLICATIONS & INFORMATION DIRECTORATE, CSIR, NEW DELHI
in association with
THE INDIAN NATIONAL SCIENCE ACADEMY, NEW DELHI

THE WEALTH OF INDIA

An Encyclopaedia of Indian Raw Materials and Industrial Products, published in two series:
(i) Raw Materials, and **(ii) Industrial Products**.

RAW MATERIALS

The articles deal with Animal Products, Dyes & Tans, Essential Oils, Fats & Oils, Fibres & Pulps, Foods & Fodders, Drugs, Minerals, Spices & Flavourings, and Timbers and other Forest products. Names in Indian languages, and trade names are provided.

For important crops, their origin, distribution, evolution of cultivated types, and methods of cultivation, harvesting and storage are mentioned in detail. Data regarding area and yield and import and export are provided. Regarding minerals, their occurrence and distribution in the country and modes of exploitation and utilization are given. The articles are well illustrated. Adequate literature references are provided.

Eleven volumes of the series covering letters A – Z have been published.

Vol. I(A-B) Rs. 80.00; Vol. II (C) Rs. 95.00; Vol. III (D-E) Rs.105.00; Vol.IV (F-G) Rs. 65.00; Vol. IV: Suppl. Fish & Fisheries Rs, 40.00; Vol. V (H-K) Rs. 75.00; Vol. VI (L-M) Rs. 90.00; Vol. VI: Suppl. Livestock Rs. 60.00; Vol. VII (N-Pc) Rs. 30.00; Vol. VIII (Ph-Re) Rs. 86.00; Vol. IX (Rh-So) Rs.104.00; Vol. X (Sp-W) Rs. 225.00; Vol. XI (X-Z) Rs. 115.00.

INDUSTRIAL PRODUCTS

Includes articles giving a comprehensive account of various large, medium and small scale industries. Some of the major industries included are: Acids, Carriages, Diesel Engines, Fertilizers, Insecticides & Pesticides, Iron & Steel, Paints & Varnishes, Petroleum Refining, Pharmaceuticals, Plastics, Ship & Boat-building, Rubber, Silk, etc.

The articles include an account of the raw materials and their availability, manufacturing processes, and uses of products, and industrial potentialities. Specifications of raw materials as well as finished products and statistical data regarding production, demand, exports, imports, prices, etc., are provided. The articles are suitably illustrated. References to the sources of information are provided.

Nine volumes of the series covering letters A – Z have been published.

Part I (A-B) Rs. 54.00; Part II (C) Rs. 64.00; Part III (D-E) Rs. 25.00; Part IV (F-H) Rs. 25.00; Part V (I-L) Rs. 30.00; Part VI (M-Pi) Rs. 28.00; Part VII (Pl-Sh) Rs. 60.00; Part VIII (Si-Ti) Rs. 66.00; Part IX (To-Z) Rs. 80.00.

HINDI EDITION: BHARAT KI SAMPADA—PRAKRITIK PADARTH

Vols. I to VI and two supplements of Wealth of India—Raw Materials series in Hindi already published.

Published Volumes:

Vol. I (अ-औ) Rs. 38; Vol. II (क) Rs. 36; Vol. III (ख-न) Rs. 36; Vol. IV (प) Rs. 83; Vol. V (फ-मेरे) Rs. 60; Vol. VI (मेल-रू) Rs. 80.

Supplements:

Fish & Fisheries (Matsya & Matsyaki) Rs. 49; Liverstock (*Pashudhan aur Kukkut Palan*) Rs. 34.

Vols. VII to XI under publication.

Please contact:
Manager (Sales & Advertisement)
PUBLICATIONS & INFORMATION DIRECTORATE, CSIR
Hillside Road, New Delhi 110012

Indian Journal of Radio & Space Physics

EDITORIAL BOARD

Prof. J C Bhattacharyya
Indian National Science Academy
New Delhi/Indian Institute of Astrophysics
Bangalore

Prof. R R Daniel
Tata Institute of Fundamental Research
Bombay

Prof. M K Das Gupta
Institute of Radio Physics & Electronics
Calcutta

Prof. H S Gurm
Panjabi University
Patiala

Dr A P Mitra
National Physical Laboratory
New Delhi

Prof. S N Mitra
Indian National Science Academy
New Delhi/Toshniwal Brothers Pvt Ltd
New Delhi

Dr Bh V Ramana Murty
Indian Institute of Tropical Meteorology
Pune

Prof. U R Rao
Indian Space Research Organization
Bangalore

Prof. R G Rastogi
Indian Institute of Geomagnetism
Bombay

Dr B M Reddy
National Physical Laboratory
New Delhi

Prof. N V G Sarma
Raman Research Institute
Bangalore

Prof. Satya Prakash
Physical Research Laboratory
Ahmedabad

Shri Y.R. Chadha, Editor-in-Chief, *Ex-officio* Secretary

EDITORIAL STAFF

Editors: D S Sastry & J Mahadevan *Assistant Editor*: N C Mondal

Published by the Publications & Information Directorate, CSIR, Hillside Road, New Delhi 110012

Editor-in-Chief: Y R Chadha

The Indian Journal of Radio & Space Physics is issued bimonthly.

The Directorate assumes no responsibility for the statements and opinions advanced by contributors. The editorial staff in its work of examining papers received for publication is assisted, in an honorary capacity, by a large number of distinguished scientists.

Communications regarding contributions for publication in the Journal should be addressed to the Editor, Indian Journal of Radio & Space Physics, Publications & Information Directorate, CSIR, Hillside Road, New Delhi 110012.

All correspondence regarding reprints, Journal copies, subscriptions, renewals, claims for missing numbers and advertisements, should be addressed to: The Sales & Distribution Officer, Publications & Information Directorate, CSIR, Hillside Road, New Delhi 110012. Payments may be sent by money order, cheque, bank draft or postal order marked payable to PUBLICATIONS & INFORMATION DIRECTORATE, NEW DELHI 110012.

Claims for missing numbers of the Journal will be allowed only if received within 3 months of the date of issue of the Journal plus the time normally required for postal delivery of the Journal and the claim.

Annual Subscription: Rs 100.00 £19.00 $ 34.00 **Single Copy**: Rs 20.00 £3.80 $ 6.80

50% Discount is admissible to research workers and students and 25% discount to non-research individuals, on annual subscription.

© 1984 The Council of Scientific & Industrial Research, New Delhi.

Indian Journal of Radio & Space Physics

VOLUME 13 NUMBER 1 FEBRUARY 1984

CONTENTS

A Study of Tropospheric Scintillations Using LOS Link at 7.6 GHz 1
H N Dutta, S K Sarkar, B M Reddy & Nandini Sengupta

Axially Symmetric Radiation Patterns from Corrugated Flanged *H*-plane Sectoral Horns... 13
P Mohanan, C K Aanandan & K G Nair

Solar Wind Interaction Region & Low Latitude Geomagnetic Field 16
G K Rangarajan & R S Ramteke

Behaviour of Space Charge Before & After Rains at a Valley Station.. 19
V N Reddy Mukku, M K Khera, A R Rafique & P N Raina

Fair Weather Atmospheric Electric Variability 24
V N Reddy Mukku, N C Varshneya & M K Khera

COMMUNICATIONS

Design, Development & Performance Evaluation of an Anechoic Chamber for Microwave Antenna Studies.. 29
E J Zachariah, K Vasudevan, P A Pravinkumar, P Mohanan & K G Nair

Phase Modulation of Microwave Signals Using Point Contact Germanium Signal Diodes .. 32
P Mohanan, C P G Vallabhan, C K Aanandan & K G Nair

Papers accepted for publication 34

Indian Journal of Radio & Space Physics
Vol. 13, February 1984, pp. 1-12

A Study of Tropospheric Scintillations Using LOS Link at 7.6 GHz

H N DUTTA, S K SARKAR & B M REDDY
Radio Science Division, National Physical Laboratory, New Delhi 110012
and
NANDINI SENGUPTA
Institute of Radio Physics & Electronics, University of Calcutta, Calcutta 700009

Received 26 *February* 1982; *accepted* 15 *November* 1983

The signal strength fluctuations at 7.6 GHz over Delhi/Sonepat line-of-sight link have been analyzed for the period 1977-78. Tropospheric scintillations have been observed to be predominantly a nightime phenomenon. Its occurrence is minimum during the monsoon season compared to any other season. The distribution of scintillation indices (SIs) indicates that around 50 % indices are below SI = 30 % and around 82 % indices are below SI = 60 %. The scintillations with SI > 60 % appear mainly during nighttime in all the seasons. The SI has been observed to be positively associated with the initial radio refractivity gradient. The fading rate is minimum during early morning hours while it is maximum during midday. The diurnal variation of C_n^2 computed from the scintillation data shows the value of C_n^2 to be minimum around midday and maximum in the nighttime. Finally, the scintillation observations have been discussed in the light of atmospheric structures observed on echosonde system.

1 Introduction

An increasing amount of interest has been focussed in recent years upon the problem of electromagnetic wave propagation in media whose properties are characterized by random fluctuations in space and time[1-3]. The atmosphere of the earth is one such medium, and this interest has been aroused both by technical pressure for more efficient utilization of the radio-through-optical spectrum, and by the recognition that the effect produced by the atmosphere upon waves propagating through it is a useful measure of the nature of the atmosphere[4-5].

When a radiowave propagates through the earth's atmosphere it is passing through a medium whose intrinsic properties are not always constant. The variations in pressure, temperature and water vapour content can alter the direction, velocity and properties of the wave. The surface of the earth acts as a curved boundary from which radio waves may be reflected and around which they may be diffracted.

Tropospheric microwave communication is strongly dependent on different modes of propagation. The three well known modes of propagation are: (i) Line-of-sight (LOS); (ii) diffraction and (iii) troposcatter. The LOS propagation is always within the horizon while the diffraction and troposcatter are beyond the horizon. The dominant mechanism in LOS propagation can be explained on the basis of two-ray-optics theory. The LOS received signal is a combination of direct ray and ground reflection with a possible contribution from scatter, etc.

Rapid variations in tropospheric signal intensity variations, usually referred to as scintillations. are caused, due to scattering, by refractive index fluctuations, consisting of irregularity structures along the path of propagation. The intensity fluctuations are measured by a well known index, namely, scintillation index (SI) adopted by AFGL and the JSSG[6]. Theoretical models describing scintillations have been verified by optical, short-hop, LOS propagation studies[7]. Staras[8] and Clifford and Strohbehn[9] have extended the theoretical models to the scintillation phenomena at microwave frequencies.

The LOS propagation through the troposphere displays a typical diurnal variation[10]. The post-sunrise and post-sunset periods are characterized by high values of SI, while the index is low and steady during daytime, when the atmosphere is convective. The high values arise because of the building up of refractivity perturbations due to layered structures in the atmosphere, which are formed after sunset, but which gradually dissipate after the sunrise. The heated air mass close to the earth's surface starts ascending after sunrise and causes considerable fluctuations in the tropospheric propagated signal. Scintillation studies afford a means of estimating Tatarskii's[11] structure parameter, C_n^2. The C_n^2 parameter gives a measure of the intensity of the refractive index irregularities existing in the atmosphere.

In this report an attempt has been made to study in detail the tropospheric scintillations over the Delhi-Sonepat LOS path of 42 km at 7.6 GHz. The data utilized refer to the period 1977-78.

2 Data Analysis

The scintillation index (SI) is defined as[6]

$$\text{SI (per cent)} = \frac{P_{max} - P_{min}}{P_{max} + P_{min}} \times 100 \quad \ldots (1)$$

where SI represents scintillation index in per cent, P_{max} is the power of the third peak down from the maximum excursion of the signal level and P_{min} denotes the power of the third minimum upwards from the minimum signal level.

The LOS data have been grouped into four seasons, namely, pre-monsoon (March-May), monsoon (June-August), post-monsoon (September-November) and winter (December-February). Refractivity profiles from radiosonde data (twice every day, one at 0000 hrs GMT and another at 1200 hrs GMT) were obtained from the India Meteorological Department at the receiving end of the microwave link, i.e. at Delhi.

The data recorded for the period 1977-78 have been utilized to calculate SI at every half hour interval resulting in 48 data points for every 24 hr of observations. An example of low SI value as calculated from the data is shown in Fig. 1(a). High SI record is shown in Fig. 1(b). It is important to mention that in the present analysis only the fluctuations above 1 dB have been referred to as scintillations while the fluctuations below 1 dB are considered to be general noise.

During the period 1977-78 the data have been recorded for 9919 hr (Fig. 2). The data in each season and the data containing scintillations are also indicated in Fig. 2. The hourly distributions of data in all the seasons are shown in Fig. 3(a-d). Each of the diagram in Fig. 3 shows the diurnal variation of the number of hours of observation containing scintillations. The diurnal variation of observations with no scintillation is also marked. It is seen that the scintillations occur round the clock with maximum occurrence being during night hours. The data containing no scintillations is maximum during monsoon compared to all other seasons representing the absence of irregularities to cause scattering for a fairly large period or it shows the atmosphere to be homogeneous.

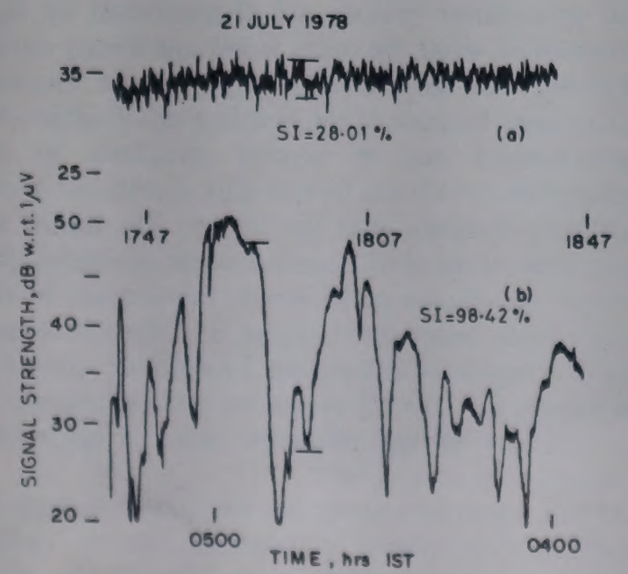

Fig. 1—Sample records showing typical signal strength variations with: (a) low SI and (b) high SI over the Delhi-Sonepat link

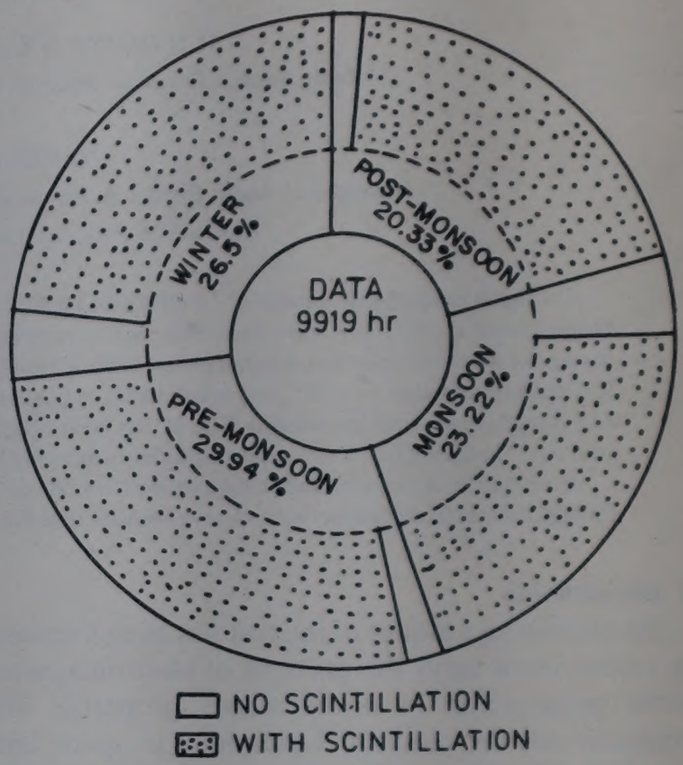

Fig. 2—Seasonwise percentage distribution of the total data analyzed for this study

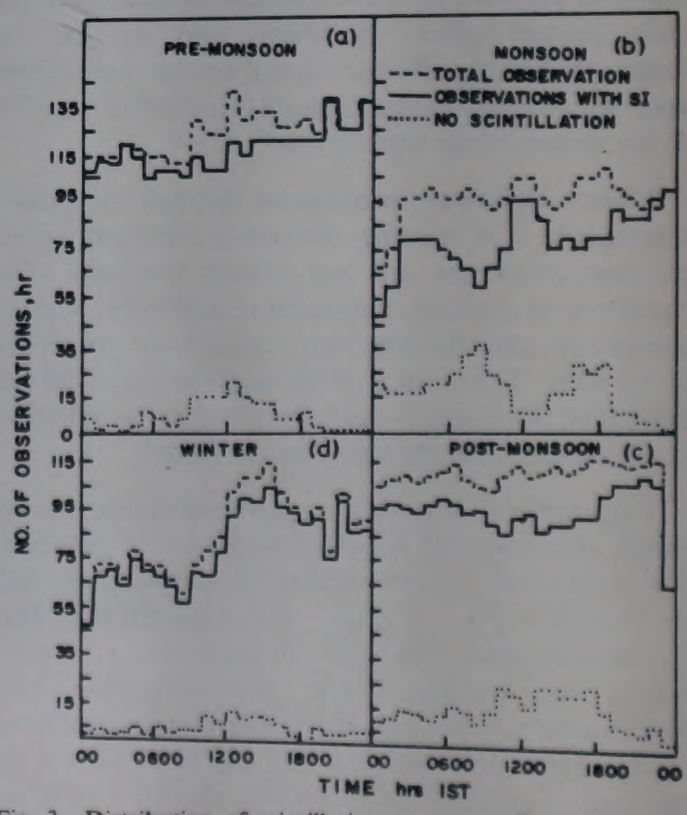

Fig. 3—Distribution of scintillation occurrence for each season, namely (a) pre-monsoon, (b) monsoon, (c) winter and (d) post-monsoon during 1977-78

3 Diurnal and Seasonal Variation

The diurnal variation of the intensity fluctuations (SI) in all the four seasons is shown in Fig. 4. Each point represents the mean SI observed during 1-hr interval and the bar indicates standard deviation. The diurnal variation shows that in general, SI is maximum at night and minimum during noon hours. At the minimum of SI during daytime, the SI is roughly the same in all the seasons indicating that under fully convective condition the atmospheric irregularities are of the same gradient. The SI is maximum in general during pre-monsoon and post-monsoon seasons and is minimum during monsoon season. The SI is roughly the same during midday in all the seasons representing the similar atmospheric conditions during this period of the day. The high value of SI during nighttime indicates the presence of high gradient irregularities in the atmosphere. It is important to note that there is, in general, a large scatter of SI in each hour and therefore the diurnal variation on an individual day may not follow the average diurnal variation as shown in Fig. 4. These typical variations have been depicted in Fig. 5. Fig. 5(a) shows an unusually steady SI from 0230 to 1730 hrs with a sharp fall in SI around 0200 hrs. Fig. 5(b) shows the low SI around nighttime and no measurable scintillation activity during daytime. Sharp changes in the SI up to 1100 hrs is another unusual SI variation observed on 15 Mar. 1977

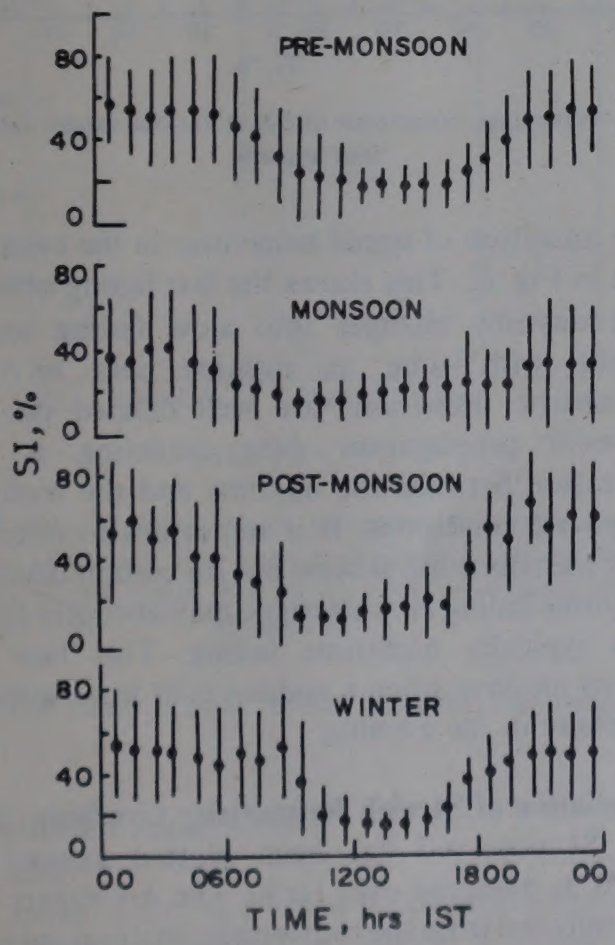

Fig. 4—Diurnal variation of SI in different seasons with the vertical bars indicating the extent of the standard deviation

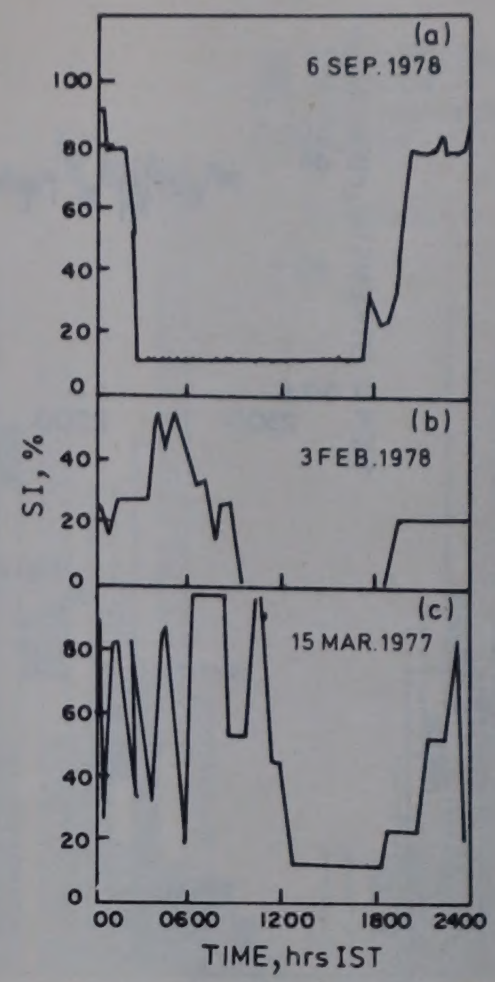

Fig. 5—Diurnal variation of SI depicting: (a) no variation in SI between 0230 and 1730 hrs; (b) no scintillations in daytime and low SI values during nighttime; and (c) large variability in SI during nighttime

[Fig. 5(c)]. This shows that the atmospheric conditions vary rapidly over a short period of time.

4 Short Bursts of Scintillations

Short bursts of scintillation as shown in Fig. 6 have been commonly observed during night hours. Such bursts persist from a few minutes to around 2 hr. The SI in such cases has been observed to vary abruptly even from SI = 10% to SI = 80%. The presence of bursts indicates that either the atmosphere becomes spontaneously unstable generating irregularities or they irregularly drift into the LOS path from other regions, but, they certainly represent regions of sharp refractivity gradients in the atmosphere.

5 Occurrence of Scintillation Indices

The percentage of occurrence of various SIs in steps of 10% is plotted in Fig. 7. It may be noted that around 50% SIs are within SI = 30% and around 82% scintillation values are below SI = 60%. The distribution of SIs in each season is represented in Fig. 8. The values are low in monsoon and around 90% of the SI values are below SI = 60%, while in winter and pre-monsoon the values are quite high. The cumulative distribution of SIs is plotted in Fig. 9. It is seen that for 25% of the time in post-monsoon the SIs are above

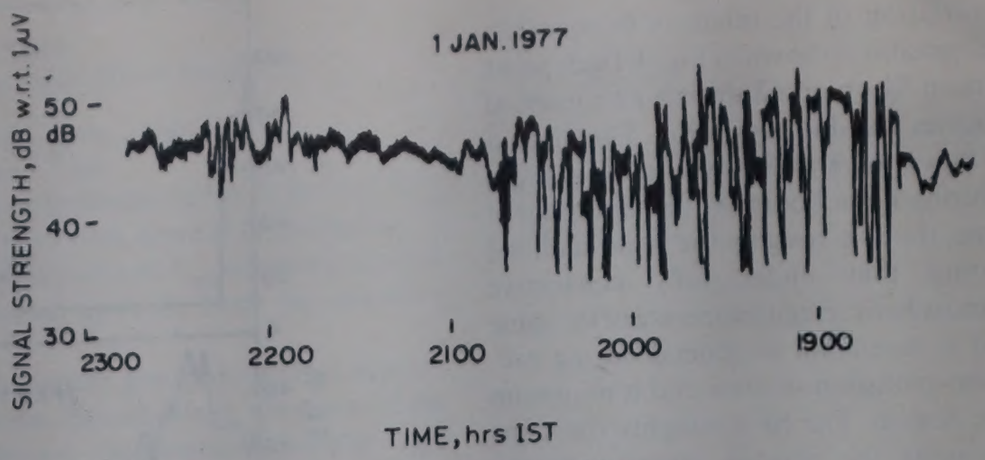

Fig. 6—Short bursts of scintillations

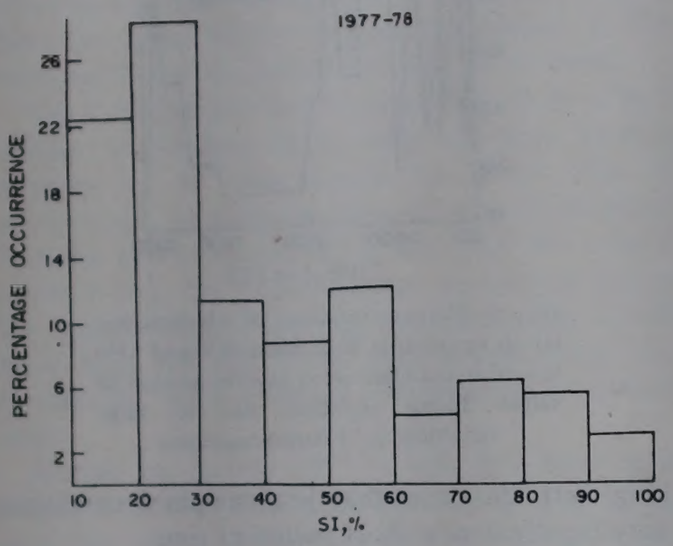

Fig. 7—Percentage distribution of occurrence of SIs in various ranges

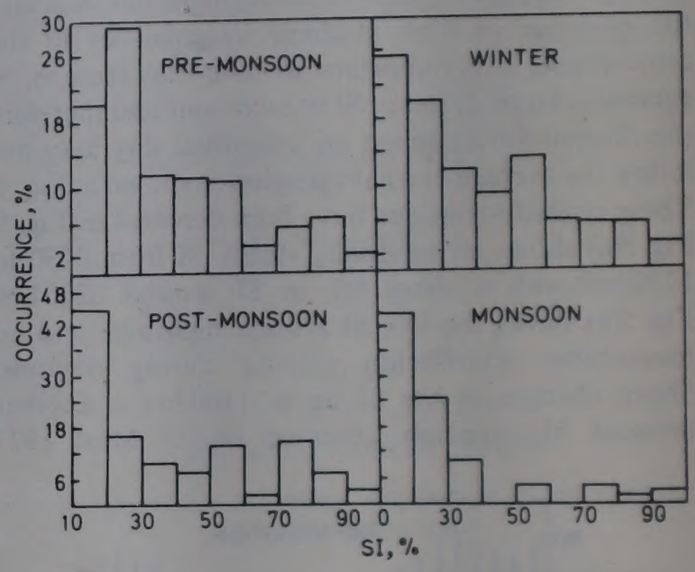

Fig. 8—Percentage occurrence of SIs in various ranges for all the four seasons

70%. At the 25% probability level the distribution shows that during winter and pre-monsoon the index is 60% which falls to 30% during monsoon. Fig. 10 presents the diurnal variation of SIs greater than 60% for 1977-78. In Fig. 10 the data refer to the 18% SI occurrence values for SI greater than 60%.It is seen that of these values, only 1.8% occur around midnight and this percentage decreases as the day advances. Practically no such value exists between 1200 and 1700 hrs. This distribution is more meaningfully represented in Fig. 11 in which the occurrence probability of SI greater than 60% in each hour has been plotted for all the four seasons. The occurrence probability is more than 30% in nighttime. The winter season has maximum occurrence of such severe scintillation. In daytime the probability is very low but as the evening sets in, the temperature falls down resulting in the formation of temperature inversion. These inversions then help in building up large scale irregularities of different air masses to persist resulting in the formation of slow and deep fades.

The transition of signal behaviour in the evening is shown in Fig. 12. This shows the fast fading observed during daytime changes into slow fading and SI increases with time as evening sets in. Such characteristic transitions are well defined on LOS microwave propagation data depicting a clear demarcation between the daytime and the nighttime atmospheric conditions. It is important to note that usually the transition is slow but on certain occasions the daytime fading characteristic may abruptly change into a typically nighttime fading. This has been observed on days when a sudden cold front grips the atmosphere in the evening.

6 Association of SI with Refractivity Gradient (ΔN)

The SI observed has been plotted against ΔN (Fig. 13), as observed over Delhi. The ΔN values have been computed from the radiosonde observation taken by the India Meteorological Department at Aya Nagar (New Delhi). The association represents a positive correlation between the two quantities:

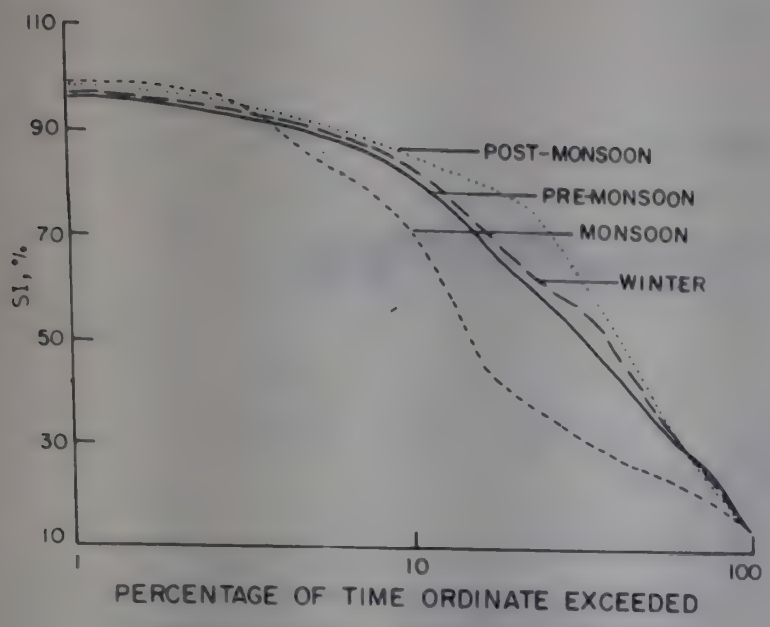

Fig. 9—Cumulative distribution of SIs

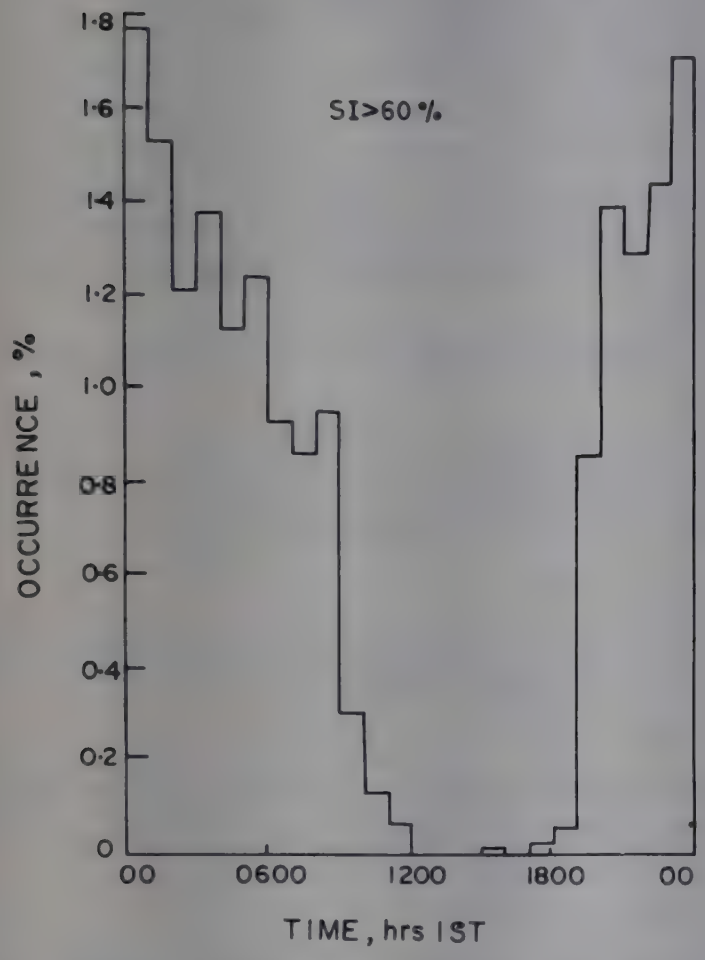

Fig. 10—Diurnal variation of the percentage occurrence of SIs >60%. (The percentage times given in the ordinate are calculated from the total time, rather than for the hours represented by the abscissae.)

however, a large scatter exists around the median curve.

7 Fading Rate Characteristics

7.1 Appearance

Fading rate of the microwave propagation signal is an important parameter to define the size of atmospheric irregularities and the limit of digital data-transmission rate. This quantity has a definite diurnal variation and examples of low and high fading rate

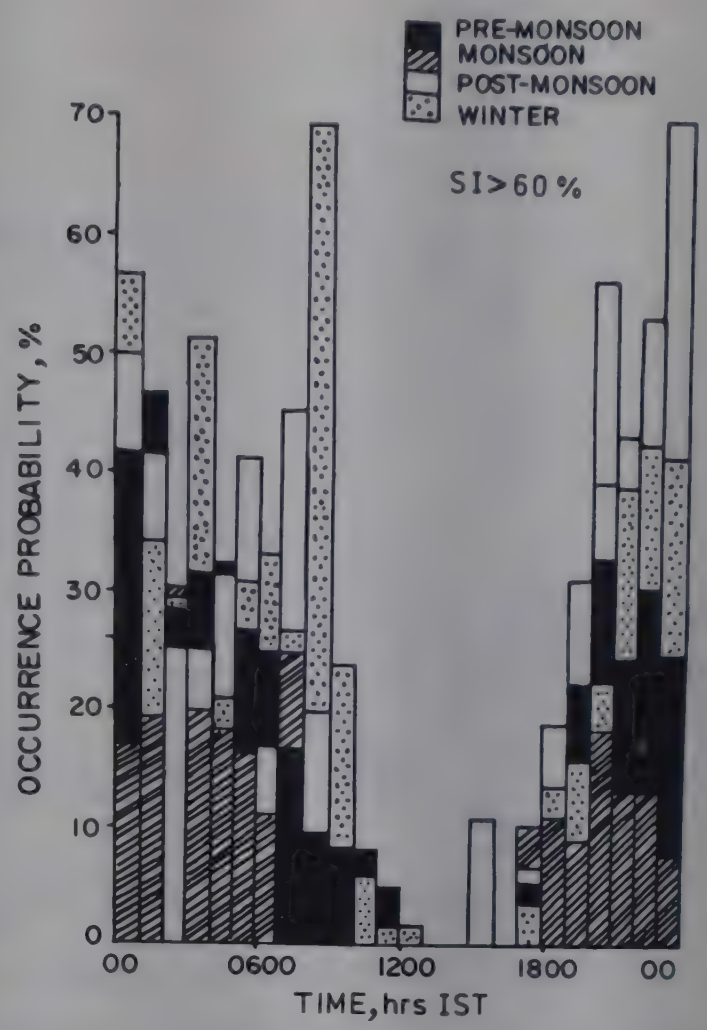

Fig. 11—Occurrence probability of SIs >60% in different seasons

illustrations are shown in Fig. 14 (a and b). Fig. 14(a) shows a slow fading signal over the Delhi/Sonepat link. The fading rate can go as low as 1 fade/hr and as high as 105 fades/hr. The fading rate has an opposite diurnal variation when compared to the SI variation. It is highest in the afternoon and minimum during early morning hours. From the highest value of fading rate in the afternoon hours it falls slowly as the evening advances and up to 2000 hrs when it attains a minimum after which it again increases with time up to 0100 hrs. The fading rate once again starts decreasing attaining a diurnal minimum between 0600 and 0700 hrs. Thus we have two minima and two maxima in each season.

Fading rate is lowest in winter compared to all other seasons. It is maximum during monsoon and post-monsoon periods. This shows that, in general, the size of the irregularities is large during winter compared to all other seasons. Also, the size of the irregularities is the largest in the early morning hours, the time when inversion has maximum gradient.

7.2 Day-to-day Variability

Fig. 15 represents the average diurnal variation of fading rate and hence the short term fluctuations are completely smoothed out. Also, the nighttime day-to-day variability is completely marked. This is

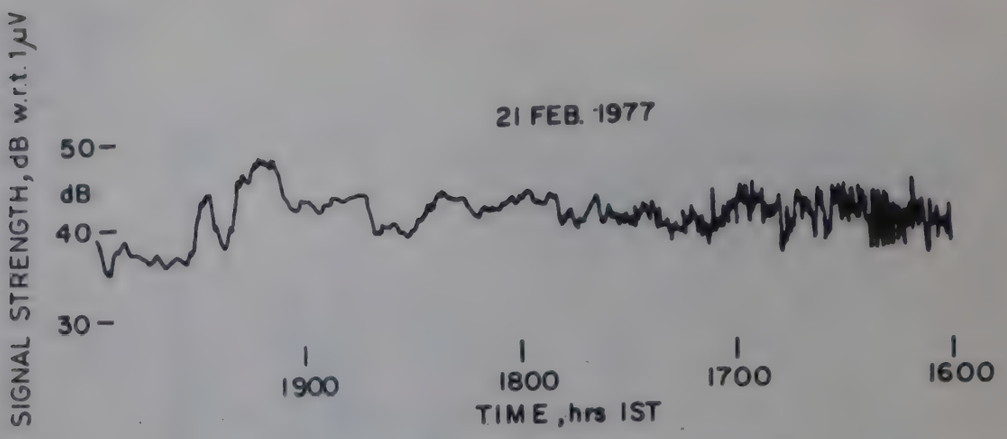

Fig. 12—Transition of signal behaviour in the evening

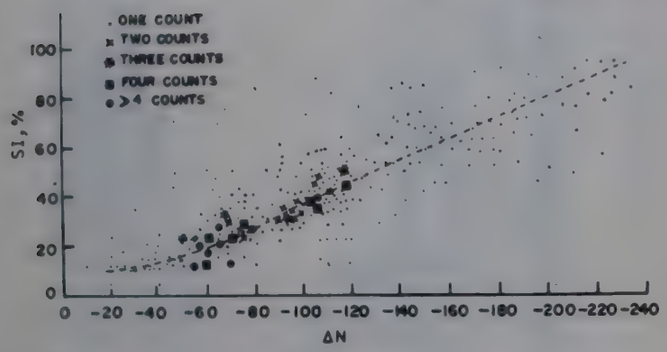

Fig. 13—Variation of SI with initial refractivity gradient

represented in Figs. 16 and 17. Fig. 16 shows the variation of fading rate during several individual nights during the period of observations. It shows a large day-to-day variability on individual nights; it also shows that an individual night may be altogether different from the average trend as seen in Fig. 15. A daytime record of unusual variation is plotted in Fig. 17. It shows a more or less steady value of fading rate from 0800 to 1700 hrs. It is important to note that like SI even the fading rate can vary greatly over a short period interval as seen in Fig. 18. This is an actual observation showing the abrupt variation of fading rate during 0500 to 0530 hrs and around 0300 to 0330 hrs.

7.3 Occurrence

The occurrence probability in per cent of fading rate during the four seasons is shown in Fig. 19. The percentage occurrence of fading rate beyond 10 is only 3 to 5 per cent, while the occurrence of fading rate between 20 and 40 is high (30-40 %, during winter). The cumulative distribution of fading rate on a seasonal basis is represented in Fig. 20. At 50 % probability level the fading rate is only 30 during the months of winter and pre-monsoon, while during monsoon and post-monsoon for 50 % of the time the fading rate is 50 fades per hour.

8 Determination of C_n^2 from Scintillation Analysis

The signal intensity fluctuations observed over a line-of-sight link are the result of the passage of refractive index irregularities over the path of the LOS link. According to Tatarskii[11], the index of refraction is an example of a random function with stationary first increments and describes its statistical properties in terms of a 'structure function'; C_n^2 (of dimension of length$^{-2/3}$) is the structure parameter of refractive index fluctuations and gives a measure of the intensity of fluctuations. In the present study of scintillations from LOS records, utilizing the computed scintillation index, C_n^2 has been calculated from the following relations.

The variance of the logarithm of the intensity is given as

$$\sigma_{\ln}^2 = \langle (\ln I/I_0 - \langle \ln I/I_0 \rangle)^2 \rangle = 4\sigma_x^2$$

this is related to the random amplitude modulation depth $m_I = \sigma_I/\langle I \rangle$, by the expression[12]

$$\sigma^2{}_{\ln} = \ln(1 + m_I^2)$$

Now m_I is equivalent to the scintillation index S_4 so the above relation can be written as

$$\sigma_{\ln}^2 = \ln(1 + S_4^2) \qquad \ldots (2)$$

There is another well known relation[11] connecting the variance with the structure parameter, C_n^2, wave number, k and path length L, viz.

$$\sigma_{\ln}^2 = 0.31\, C_n^2\, k^{7/6}\, L^{11/6} \qquad \ldots (3)$$

Combining relations (2) and (3) C_n^2 has been computed. Fig. 21 gives a diurnal and seasonal plot of C_n^2. During the early morning hours the pre-monsoon values of C_n^2 are high, whilst during evening hours the post-monsoon values of C_n^2 are higher.

It is important to note that the diurnal variation of C_n^2 can be computed only from the data where scattering is predominant. In case of layers during nighttime, the signal at the receiving end is predominantly due to the reflection from the inversion layers and the scattering portion is low. Under such circumstances the C_n^2 computation has no meaning and as such the derived values during night are fictitious. To solve this problem the data containing only the severe scintillation activity with high fading

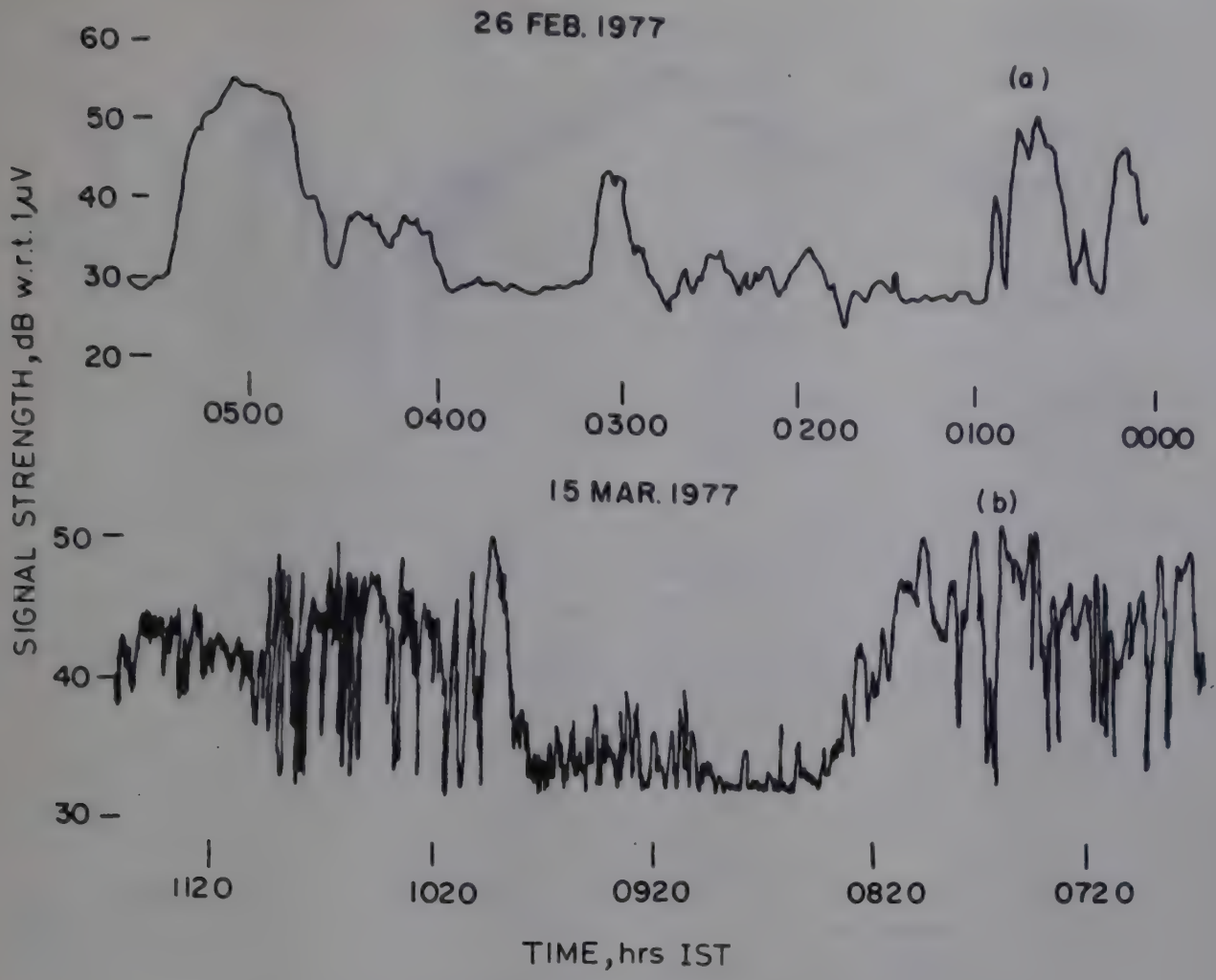

Fig. 14—Examples of low (a) and high (b) fading rates observed over Delhi/Sonepat link

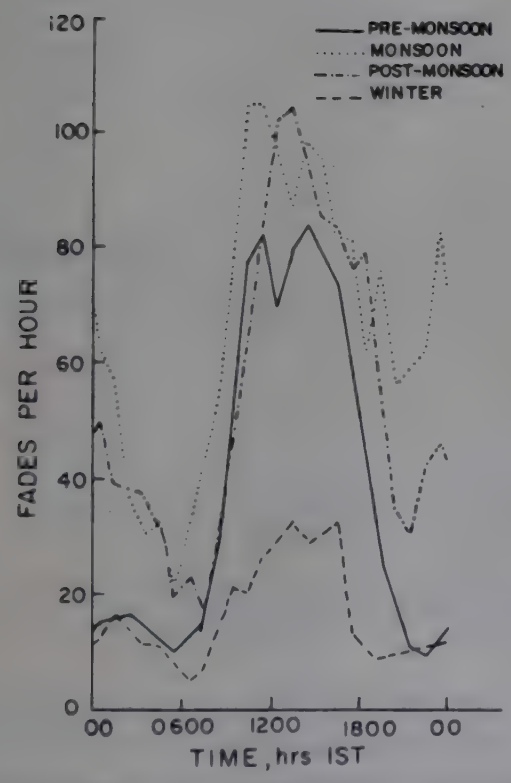

Fig. 15—Diurnal variation of average fading rate

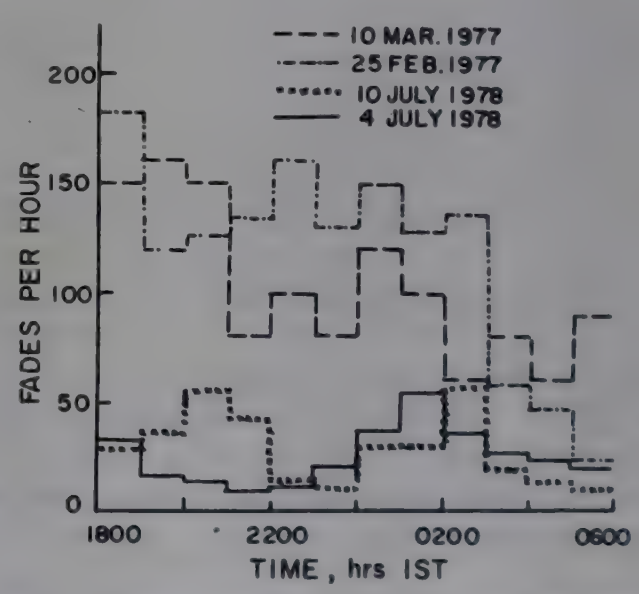

Fig. 16—Day-to-day variability in the nocturnal variation of fading rate

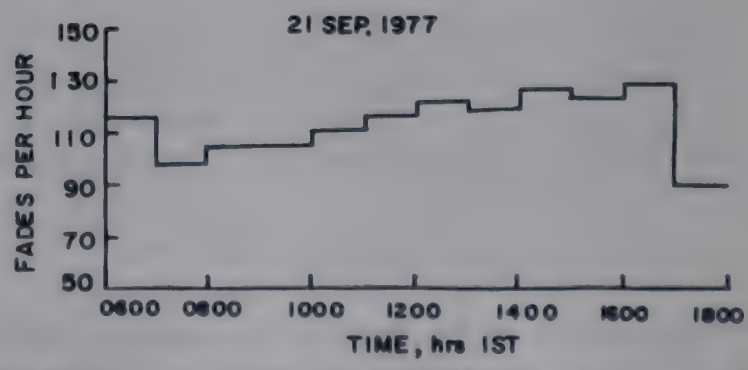

Fig. 17 Variation of fading rate during daytime as observed on 21 Sep. 1977

rate have to be utilized. The variation of C_n^2 computed from the scattering data should be more realistic than computing from the usual data.

9 Determination of C_n^2 from Power Spectrum Analysis

The structure parameter C_n^2 has also been computed from the power spectra of the scintillation records,

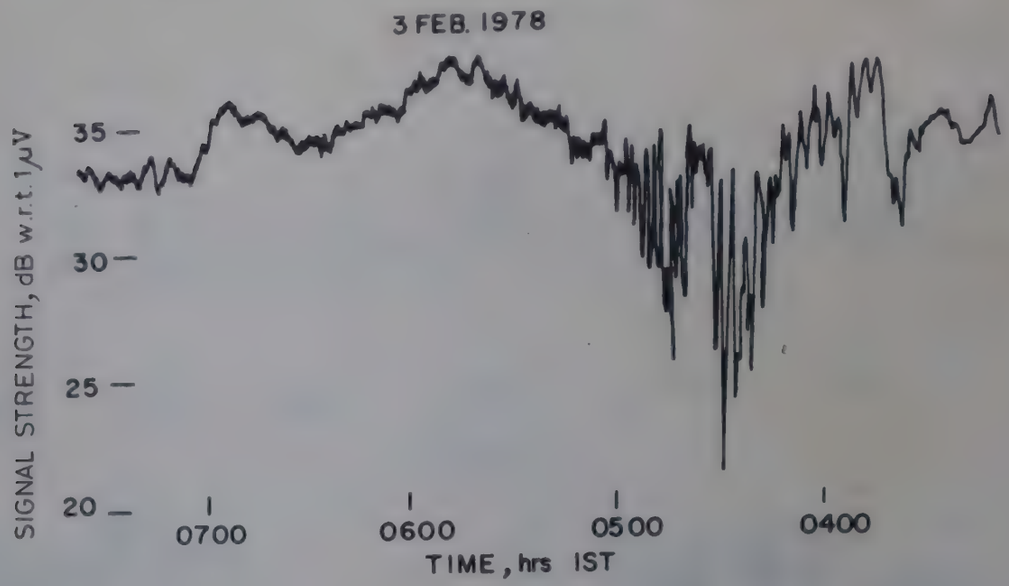

Fig. 18—Unusual rapid variation of fading rate in a short interval of time

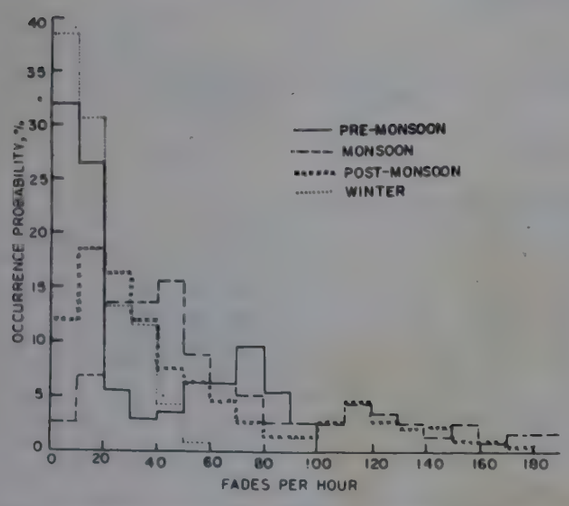

Fig. 19—Occurrence probability of fading rates in all the seasons

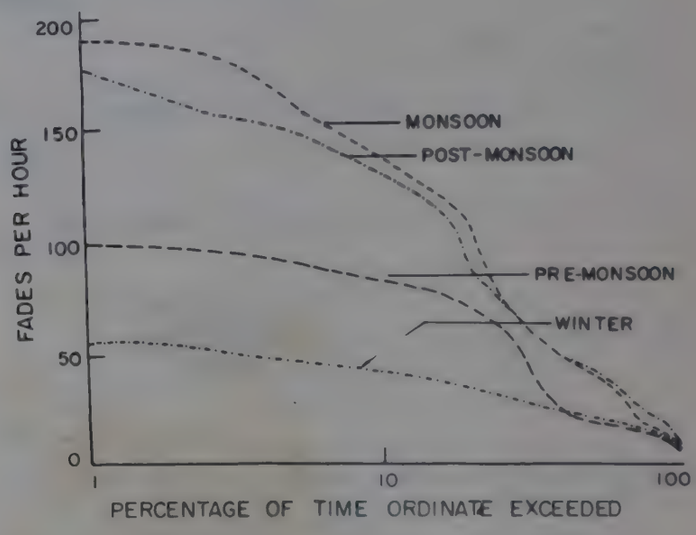

Fig. 20—Cumulative distribution of fading rates

using the fast Fourier transform (FFT) algorithm[10,13-15]. The theoretical formulations of the temporal intensity spectra for a radio wave propagation through a turbulent medium has been given by Ishimaru[16] as

$$P_I(f) \propto \begin{cases} C_n^2 & f < f_c \\ C_n^2 (f/v)^{1-|m|} & f > f_c \end{cases}$$

where m is the exponent in the power law expression for the spatial wave number spectrum, v the mean drift (wind) speed of the fading medium transverse to the radio path, and f_c a critical breakpoint frequency, given by

$$f_c = (2\pi)^{-1.2} v (\lambda L)^{-1/2}$$

If we denote the amplitude of the spectrum at f_c to be $P_I(f_c)$, from the computed power spectrum; then the structure parameter C_n^2 is given by[16]

$$C_n^2 = P_I(f_c)(2\pi \times 0.033)^{-1} \times v k^{-(5-|m|)/2} L^{-(1+|m|)/2} \times \left[\frac{\pi}{4\Gamma\{(3+|m|)/2\} \sin\left\{\left(\frac{\pi}{4}\right)(5-|m|)\right\}} \right]^{-1} \times \left[\left(\frac{|m|+1}{2}\right) \cdot \Gamma^2 \left\{ \frac{(|m|+1)/2}{\Gamma(|m|+1)} \right\} \right]^{-1}$$

When we consider the case of layered stratification in the atmosphere, specifying C_n^2 has no physical significance[17]; C_n^2 associated with layered structures is entirely fictitious. In any case comparing the structure parameter with those obtained from the logamplitude fluctuations of the scintillation records, we have found that both the methods given in Sections 8 and 9 give the same order of magnitude of C_n^2. Fig. 22 gives a power spectral density plot for morning hours, C_n^2 has been computed as 3.18×10^{-12} ($m^{-2/3}$) for a spectral slope of $m = -9.36/3$.

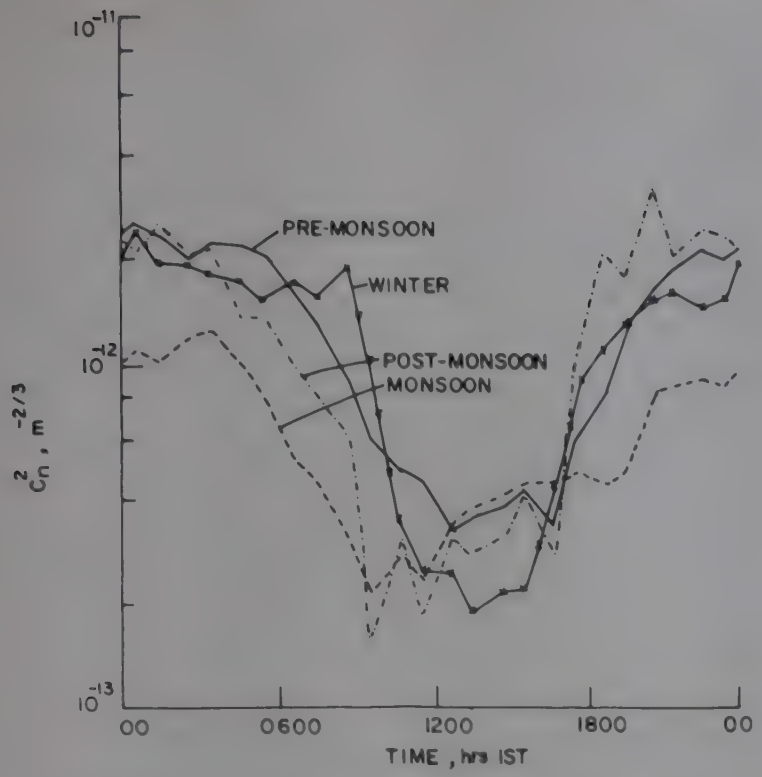

Fig. 21—Seasonal and diurnal variation of average C_n^2

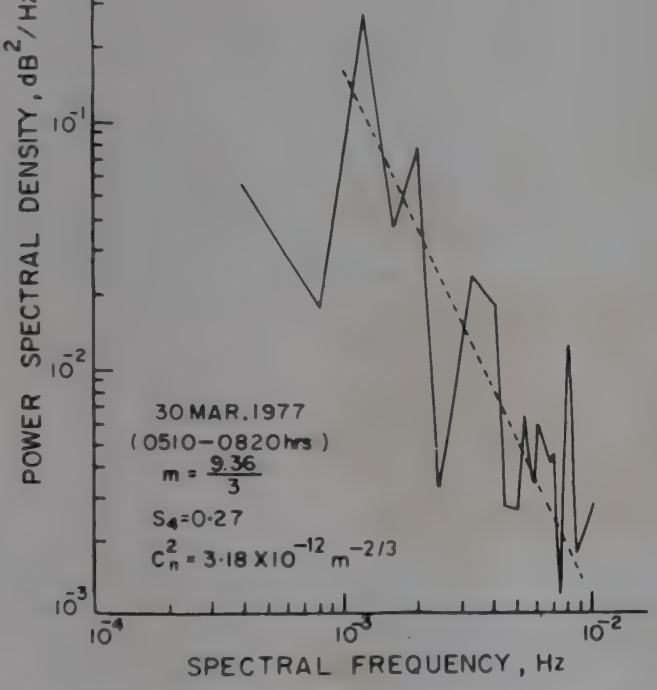

Fig. 22—Power spectral density plot for morning hours on 30 Mar. 1977

10 Discussion

It is well known that during daytime the atmosphere usually consists of thermal plumes because of earth's surface heating. Simultaneous microwave amplitude measurements show rapid fluctuations of 1 to 2 dB and the signal remains fairly steady. It has been observed that during daytime, the scintillation index which is a measure of fading depth does not vary appreciably because during this period the refractivity gradient derived from radiosonde measurements also show less variability. But, during nighttime, the variation in

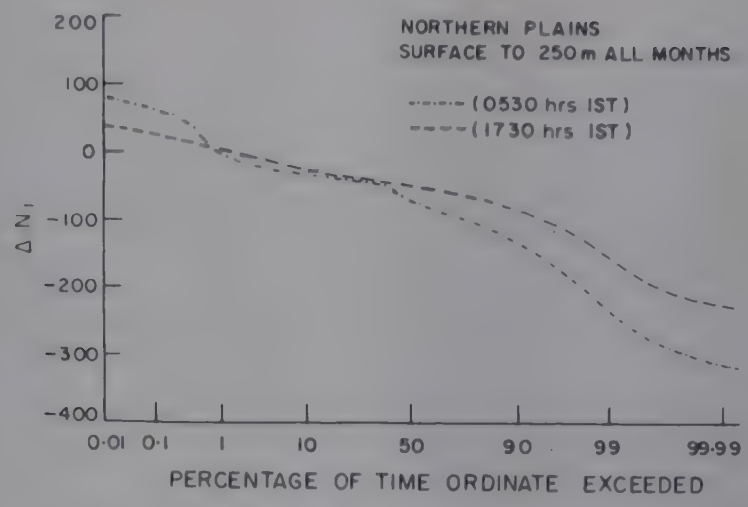

Fig. 23—Cumulative distribution of refractivity gradient over northern plains for 0530 hrs and 1730 hr IST

refractivity gradient is large compared to daytime as shown in Fig. 23. SIs observed during nighttime also show large variation because during nighttime climatic conditions over the plains of Northern India also have large variability. However, the results reported earlier over the Indian East Coast[18], it was found that even during daytime SI varied appreciably. This is because, over the coastal region, humidity varied from day to day which ultimately affects the microwave propagation in a different way.

It is seen that over Delhi during daytime the refractivity gradient (ΔN) for 90% of the time is of the order of $-50N$/km which characterizes that the lower atmosphere is well mixed. The fading rate observed during daytime is also found to be low which clearly indicated that during this period the microwave amplitude variation is associated with the scattering phenomena. During nighttime, the fading rate is of low order but the variability is more which clearly shows that during nighttime the propagation characteristics is associated with different situations like scattering and reflection. The distribution of refractivity gradient during morning hours varies from $-40N$/km to $-200N$/km which clearly indicates that during nighttime over Delhi all the different climatic situations like sub-refraction, super-refraction and ducting prevail.

Also, the variability can be best seen from acoustic sounding data taken over Northern Plains (Patiala) of this country. In daytime the atmosphere is characterized by the appearance of thermal plumes; the convective flow of air (Fig. 24). However, deviations from the well defined convective flow are observed due to high wind fog/rain and structures due to cold fronts. The heavy air flow distorts the convective cells. Rain can change the atmosphere from convective to homogeneous and if the temperature drops still further, even inversion can be generated and a daytime structure may be transformed into a nighttime structure. A cold front can certainly cause the elevated

structures to form in the atmosphere, as a cold front is a sloping layer in the lower atmosphere marking a transition in temperature (density) which in pronounced cases extends from the earth's surface to tropopause with colder air underlying the warmer. The slope is of the order of 1 : 100 in the lower troposphere becoming gradually steeper in the upper troposphere. The vertical depth of frontal layer is of the order of 1 km, and horizontal width is of the order of 100 km. There is also a rapid transition across a frontal zone of the wind component parallel to the front, forming a cyclonic wind shear. Besides temperature and wind contrasts, fronts also carry typical clouds and precipitation system indicating the existence of vertical circulation. But as the front is associated with high winds, it becomes a phenomenon for a duration of the order of an hour or two to affect the propagation characteristics and SI under such circumstances can be high.

The convective flow diminishes slowly as night approaches and on echosonde we can clearly study such evening transitions. The convective flow is transformed slowly into a ground-based inversion and the fading characteristics of the LOS microwave propagation data clearly show such transitions (Fig. 12).

The nighttime atmospheric structures have a high degree of variability. The presence of a ground-based layer, variable in thickness, and the appearance of highly variable elevated layers; the wave motions within and above the inversions; and turbulence—all these contribute maximum towards the atmospheric

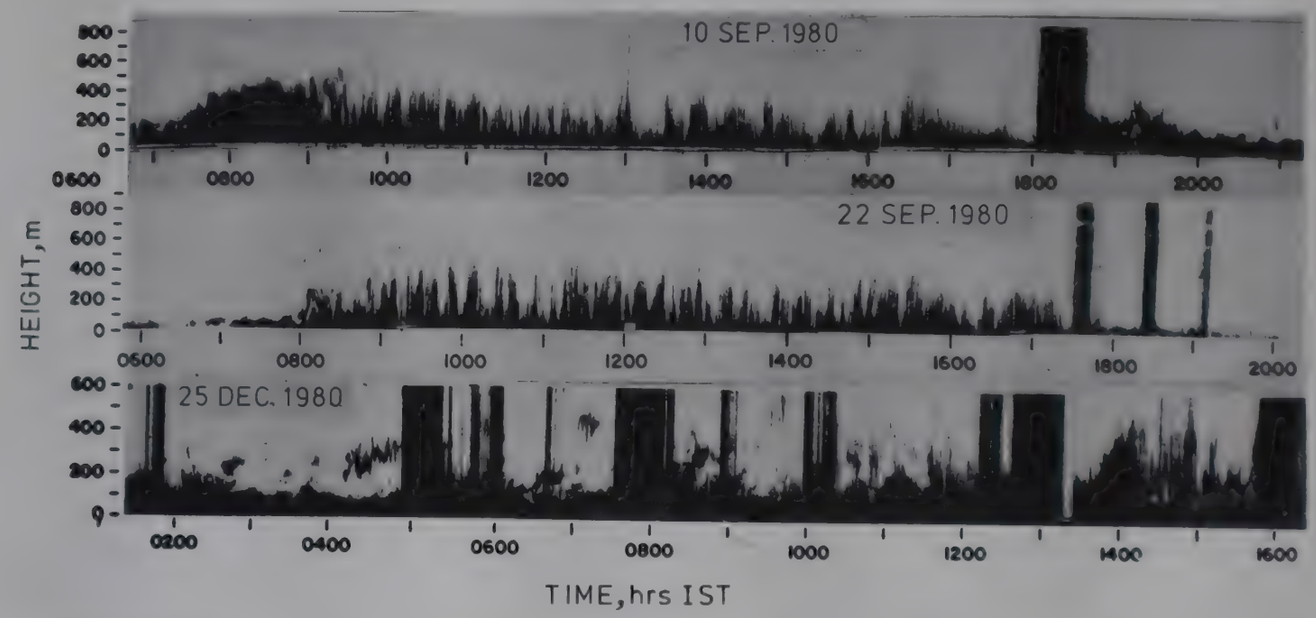

Fig. 24—Daytime echograms depicting well-defined convection (10 Sep. 1980 and 20 Sep. 1980) and presence of inversions and fronts on a cloudy and a rainy day

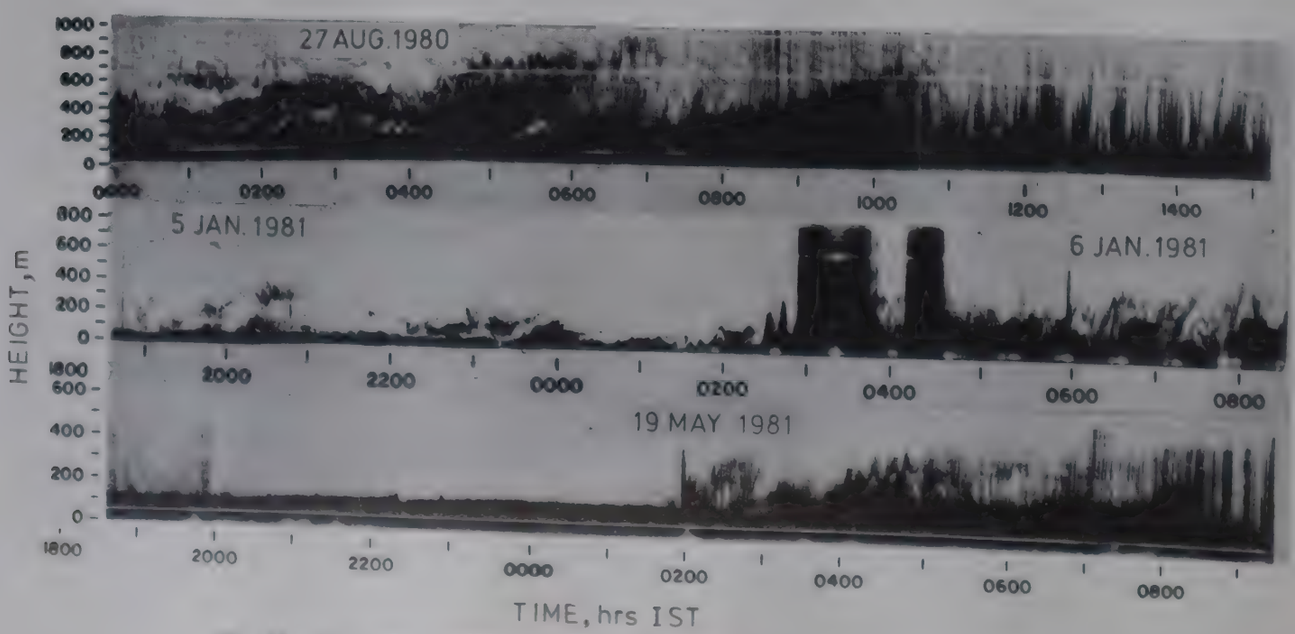

Fig. 25—Nighttime echograms depicting variability of the dynamics of inversions

variability at night (Fig. 25). Moreover, the ground level inversion itself helps in the persistence of irregularities. In daytime convection breaks the irregularities into small-scale irregularities and hence the variability is low.

A brief review of the computation of C_n^2 by several workers is worthwhile in connection with the present study of scintillation analysis of LOS records. A typical value of C_n^2 for $n=11/3$ from power spectrum analysis is $8\times10^{-14}\mathrm{m}^{-2/3}$ corresponding to a mean height interval of 1 km[10,17]. Tatarskii[11] evaluated C_n^2 at 1.5 km to be in the range 1.4×10^{-13} to $4.4\times10^{-16}\mathrm{m}^{-2/3}$. Gjessing[19] considered a value of $C_n^2=2.2\times10^{-11}$ to be a typical estimate. Clifford and Strohbehn[9] quoted $C_n^2=4\times10^{-14}\mathrm{m}^{-2/3}$ for calculating optical variance. Majumdar[20] quoted C_n^2 to be 10^{-13} to $10^{-14}\mathrm{m}^{-2/3}$ to be consistent with spectral slope of $-13.5/3$ to $-15/3$ in transmission loss data. In the present study by power spectrum analysis, we have obtained a value of $3.18\times10^{-12}\mathrm{m}^{-2/3}$ for C_n^2 corresponding to a slope of $-9.36/3$.

The height dependence picture of C_n^2 values would be a more revealing state of the atmosphere. However, this cannot be formed from a limited set of values quoted by different authors. The physical parameter to look upon for height dependence is the variance of refractive index fluctuations $\langle(\Delta n^2)\rangle$. No consistent results are available on the height dependence of $\langle(\Delta n^2)\rangle$ (Ref. 19-21). Wesley *et al.*[22] has computed the diurnal cycle of C_n^2 from the estimates of sensible and latent heat flux components of the surface energy budget. Diurnal and seasonal variation of C_n^2 have been calculated for 0.5, 2, 8 and 16 m above the ground. The diurnal variation exhibits two minima and three peaks. However, since the LOS path passes over a height of 80 m, it is not justifiable to compare the diurnal variation of C_n^2 obtained from LOS records in this study with those of Weslely *et al.*[22] Firstly, since the method employed is different and also the height at which C_n^2 has been computed is too low.

11 Conclusions

(i) LOS microwave signals provide continuous monitoring of the atmosphere and reveal several atmospheric features.

(ii) The scintillation activity has a definite diurnal variation with maximum activity during 2100 to 0300 hrs and minimum during 1100 to 1600 hrs.

(iii) The SI is lower in general during monsoon compared to other seasons; however, the daytime scintillation activity is approximately the same in all the seasons.

(iv) Short burst of scintillation is basically a nighttime phenomenon representing the atmospheric variability. The short burst of scintillation may represent that the atmosphere becomes spontaneously unstable for a short period generating irregularities or the atmospheric irregularities are drifted into the line-of-sight path of propagation.

(v) The percentage occurrence of scintillation indices shows that around 50% values are below SI = 30% and only around 5% values are above SI = 60%.

(vi) The probability of occurrence of SI = 60% is only 1.8% at night around midnight and no such SI value has been observed during 1200 to 1700 hrs.

(vii) The evening of fades per hour has a definite pattern. It is maximum during daytime and minimum during early morning hours. The fading rate is low in general during winter compared to any other season.

(viii) The scintillation index bears a positive correlation with the initial refractivity gradient.

(ix) An estimation of C_n^2 shows a diurnal variation with high values during nighttime and low values during daytime. However, these values are fictitious since C_n^2 values computed from layered structures during nighttime because the signal is predominantly due to reflection from inversion layers. To solve this problem diurnal variation of C_n^2 has been computed from scattered data.

(x) C_n^2 estimation has also been made using the power spectrum analysis and for a spectral slope of $m=-9.36/3$ it has been estimated to be $3.1\times10^{-12}\,\mathrm{m}^{-2\,3}$.

(xi) The discussion of the scintillation data reveals that the atmospheric variability is higher during nighttime compared to daytime. This has been confirmed using the radiosonde and echosonde data.

References

1 Sarkar S K, Ramakrishna M, Dutta H N, Pasricha P K, Reddy B M, Bandyopadhay P, Chatterjee S K & Sengupta Nandini, *J Inst Telecommun Eng (India)*, **27** (1981) 277.

2 Lane J A, *J Atmos & Terr Phys (GB)*, **21** (1961) 157.

3 Pasricha P K, Sarkar S K, Banerjee P K & Ramakrishna M, *J Inst Telecommun Eng (India)*, **25** (1979) 240.

4 Kirby R S, Dougherty H T & McQuate P L, *Proc IRE (USA)*, **43** (1955) 1467.

5 Sarkar S K, Ramakrishna M, Dutta H N & Reddy B M, *Centrop Rep. No. 35, National Physical Laboratory, New Delhi, India*, 1981.

6 Whitney H E, Aarons J & Maliki C, *Planet & Space Sci (USA)*, **17** (1969) 1069.

7 Strohbehn J W, *Boundary Layer Meteorol (USA)*, **4** (1973) 397.

8 Staras H, *J Appl Phys (USA)*, **23** (1952) 1152.

9 Clifford S F & Strohbehn J W, *IEEE Trans Antennas & Propag (USA)*, **18** (1970) 264.

10 Sarkar S K, *Radioclimatological effects on tropospheric radiowaves propagation over the Indian subcontinent*, Ph D thesis, Delhi University, Delhi 1978.

11 Tatarskii V I, *The effect of the turbulent atmosphere on wave propagations*, Nauka, 1971.

12 Andreyev G A & Chernaya L F, *Telecommun & Radio Eng Part 2 (USA)*, 33 (1978) 64.

13 Otnes R K & Enochgon L, *Digital time series analysis*, (John Wiley & Sons), 1972.

14 Brigham E O, *The fast Fourier transform* (*Englewood Cliffs Prentice Hall*) 1974.

15 Pasricha P K, *A study of equatorial ionospheric scintillation at 327 MHz*, Ph D thesis Delhi University, Delhi, 1977.

16 Ishimaru A, *IEEE Trans Antennas & Propag* (*USA*), **20** (1972) 10.

17 Pasricha P K, Sarkar S K, Banerjee P K & Ramakrishna M, *J Electron & Telecommun Eng* (*India*), **25** (1979) 240.

18 Sarkar S K, Ramakrishna M, Dutta H N, Reddy B M & Sengupta Nandini, *Centrop rep. No.* 33, *National Physical Laboratory, New Delhi*, 1980.

19 Gjessing D T, *Radio Sci* (*USA*), **4** (1969) 1195.

20 Majumdar S C, *Transhorizon propagation characteristics over the Indian subcontinent*, Ph D thesis, Calcutta University, Calcutta, 1974.

21 Lane J A, *Proc IEEE* (*USA*), **115** (1968) 1227.

22 Wesley M L & Alcaraz E C, *J Geophys Res* (*USA*), **78** (1973) 6224.

Indian Journal of Radio & Space Physics
Vol. 13, February 1984, pp. 13-15

Axially Symmetric Radiation Patterns from Corrugated Flanged *H*-plane Sectoral Horns

P MOHANAN, C K AANANDAN & K G NAIR
Department of Electronics, University of Cochin, Cochin 682 022

Received 26 *March* 1983; *revised received* 28 *October* 1983

A modified *H*-plane sectoral horn antenna with identical *E*- and *H*-plane patterns over the X-band frequency is discussed. This system has significantly reduced side lobes and back lobes. Half-power beam width and gain of the antenna are also improved with enhanced matching. Experimental results for a number of horns with various flanges are presented. These find practical application for illuminating symmetric antennas like paraboloids and polarization measurements in radio astronomy, etc. Compared to the fixed pyramidal horns, the present system offers great convenience in trimming the antenna characteristics.

1 Introduction

Many workers reported that a *H*-plane sectoral horn with corrugated flange can have a beam with adjustable characteristics[1]. It is established that conducting corrugated flanges satisfying certain optimum conditions are very effective, and produce identical *E*- and *H*-plane patterns in an *E*-plane sectoral horn[2]. But the effect of corrugated flanges in *H*-plane sectoral horn for symmetric radiation patterns is not presented so far. This paper deals with such a phenomenon. It is believed that a corrugated flange with corrugation edges perpendicular to the *E*-vector will not modify the *H*-plane radiation pattern. But from the experimental results, it is clear that it can modify the *H*-plane radiation pattern also.

Fig. 1 shows the geometry of the corrugated flanged *H*-plane sectoral horn. The flanges are mounted with their corrugation edges perpendicular to the *E*-vector. The width of the flange is greater than the wavelength used, and nearly equal to 3λ. The height h, of the corrugation is of the order of $\lambda/4 < h < \lambda/2$ to prevent surface waves[3]. The slot walls are vanishingly thin compared to the slot width. The antenna system is excited by using microwaves at X-band generated by a Gunn-diode, where the propagation is in the TE_{10} mode. The *E*- and *H*-plane radiation patterns of various corrugated flanges with different parameters, at the optimum on-axis power density positions are plotted using an automatic antenna turn-table and recorder in an anechoic chamber as mentioned in Ref. 3.

2 Experimental Results & Discussion

It is observed that depending upon the position of the flange from the aperture, Z, we get maximum and minimum on-axis power density. The position giving maximum value of on-axis power density is called 'O' position and the other 'M' position[4]. So, for a particular horn with fixed flange parameters, there are more than one 'O' positions. A flange at the 'O' position gives a sharp beam in the *E*-plane with low side lobes. In the 'M' position, it gives a split beam[1]. It is observed that a symmetric radiation pattern is possible only when the flange is in the second optimum position from the aperture of the horn. In the first optimum position, it is noted that the *E*-plane half-power beam width is less than the *H*-plane. Optimizing the corrugation periods (N) flange angle (2β), etc. we can produce symmetric radiation patterns.

Fig. 2 shows the dependence of VSWR and normalized on-axis power with the position of the flange from the aperture of the horn. At the second optimum position (O_2) where the pattern is axially symmetric (Fig. 2), the VSWR of the system is less than the natural horn (i.e. horn without flanges) with enhanced on-axis power. Fig. 3 shows typical radiation patterns of a flanged *H*-plane sectoral horn at 9.5 GHz. Natural radiation patterns of the horn are also shown for comparison in Fig. 4. The natural half-power beam

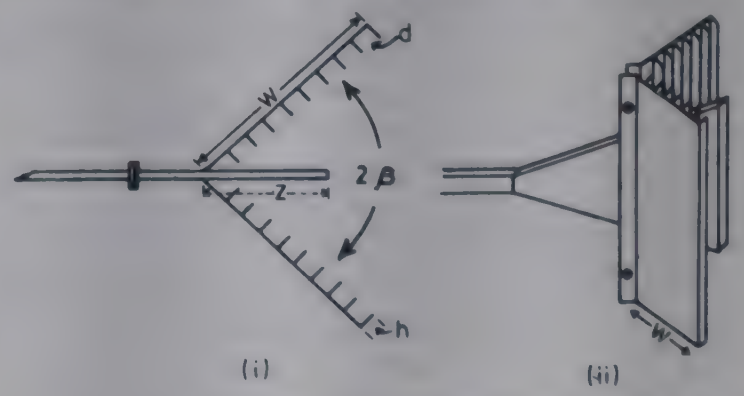

Fig. 1—Geometry of the flanged *H*-plane sectoral horn [(i) *E*-plane view (W = width of the flange, d = corrugation width, h = corrugation depth); and (ii) *H*-plane view]

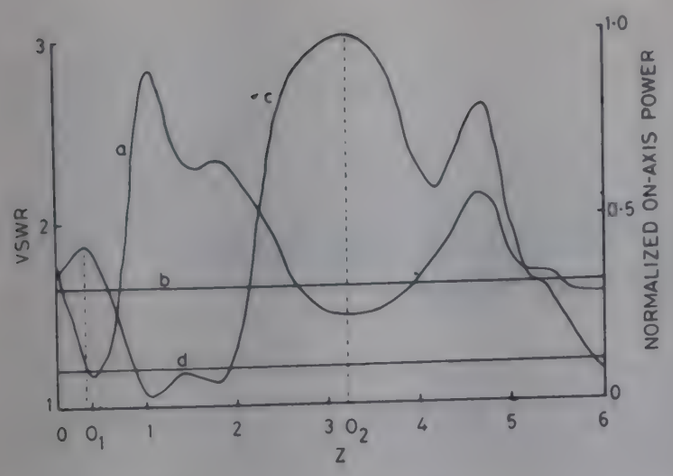

Fig. 2—Variation of VSWR and normalized on-axis power with the position of the flange from the aperture (z) at frequency 9.5 GHz, $2\beta = 60°$ and $N = 9$ [(a) VSWR with flange; (b) natural VSWR of the horn; (c) on-axis power with flange; (d) natural on-axis power of the horn; O_1, the first optimum position; and O_2, the second optimum position]

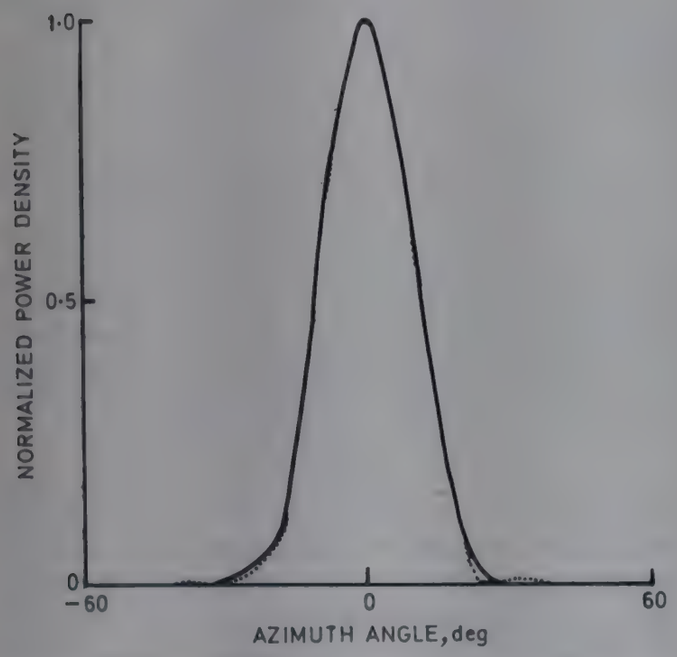

Fig. 3—Radiation patterns of flanged *H*-plane sectoral horn at 9.5 GHz for $z = 3.2$. $2\beta = 60°$ and $N = 9$ (....., *H*-plane; ——, *E*-plane)

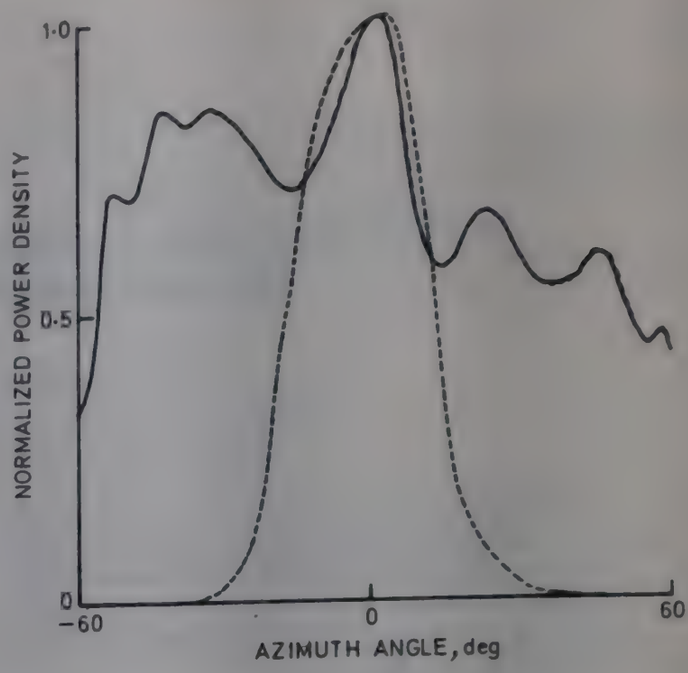

Fig. 4—Natural radiation patterns of the *H*-plane sectoral horn (without flanges) at 9.5 GHz (-----, *H*-plane; ——, *E*-plane)

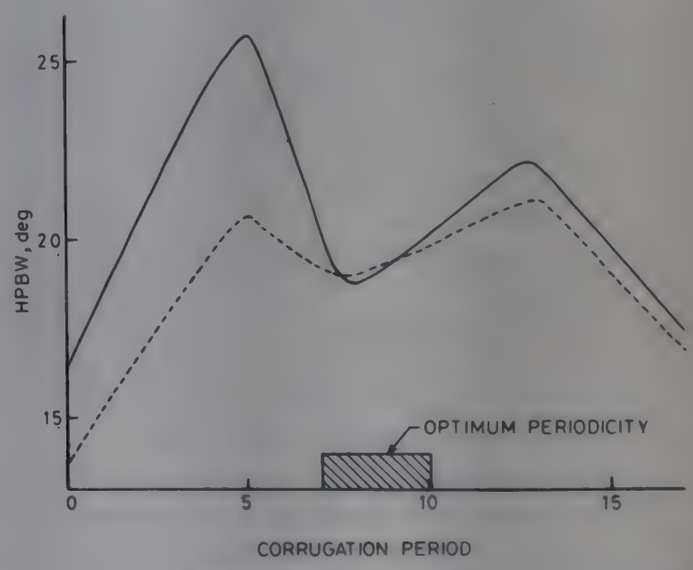

Fig. 5—Variation of HPBW with corrugation period when the flange is kept at the optimum position at 9.5 GHz and $2\beta = 60°$ (-----, *H*-plane; ——, *E*-plane)

width (HPBW) in *E*- and *H*-plane are 91.56° and 28.09°, respectively. With flanges in the second 'O' position (Fig. 3) it becomes 20.19° each. The first sidelobe level of the system at 9.5 GHz is −23.63 dB. The modification of the *H*-plane radiation pattern can be qualitatively explained as follows. The tips of the corrugations act as an array of linear antennas. A point in the *H*-plane, the contribution from the aperture of the horn and this array are considered. This effectively modifies the *H*-plane radiation pattern. The variation of on-axis power density with flange position can also be explained. The distance between the aperture of the horn and this effective array is varied as we move the flange from the aperture. Depending upon the distance, we can obtain an end-fire (sharp beam along the on-axis) or broadside (split beam), etc.

Fig. 5 gives the variation of the HPBW in both the planes with corrugation periods at 9.5 GHz. It is evident from Fig. 5 that a symmetric radiation pattern is possible only for a critical region. This region is marked as optimum periodicity region in Fig. 5. Shown in Fig. 6 is the dependence of the HPBW on flange angle. Again, symmetric pattern is obtained when the flange angle is 60° for this typical case. The dependence of HPBW on frequency is shown in Fig. 7. Over the frequency range of 8-11 GHz, the two beam widths virtually go together. Variations of antenna gain with corrugation period and frequency are given in Tables 1

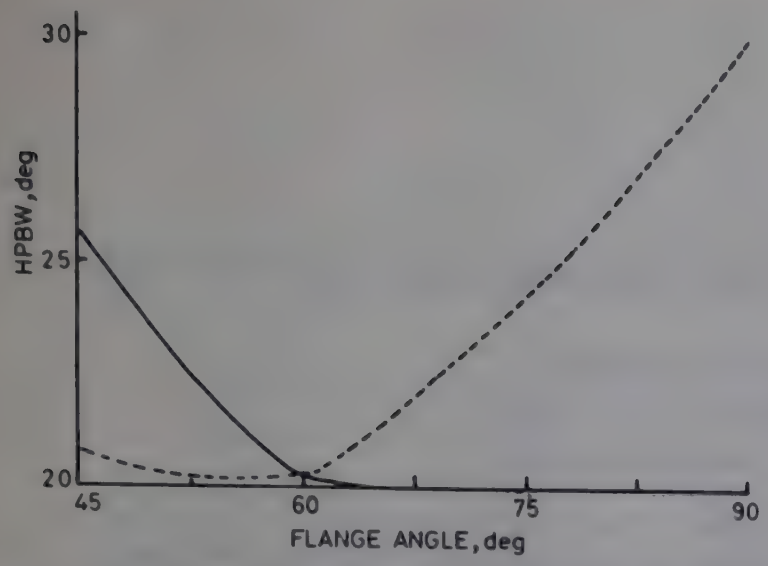

Fig. 6—Variation of HPBW with flange angle when the flange is kept at the optimum position at 9.5 GHz and $N=9$ (-----, *H*-plane; ——, *E*-plane)

Table 1—Variation of Antenna Gain with Corrugation Period (Frequency = 9.5 GHz, $2\beta = 60°$)

Period of corrugation	*E*-plane gain dB	*H*-plane gain dB
17	19.54	19.78
13	23.64	21.28
9	22.18	23.88
7	21.50	21.70
5	21.54	23.12
Natural horn	6.10	23.18

Table 2—Variation of Antenna Gain with Frequency ($2\beta = 60°$, $N=9$)

Frequency GHz	*E*-plane gain dB	*H*-plane gain dB
8.2	20.64	20.28
8.5	27.46	27.80
9.0	20.44	20.68
9.5	20.70	20.52
10.0	23.12	21.98
10.5	25.30	26.52
11.0	23.74	22.12
11.2	24.72	27.18

and 2, respectively. The gain is calculated from the radiation patterns. The natural *H*- and *E*-plane gains are also given for comparison. The gain is found to be constant over the entire frequency band. Considerable improvement in gain is noted with corrugated flanges.

3 Conclusion

It is established that conducting corrugated flanges satisfying certain critical conditions will give

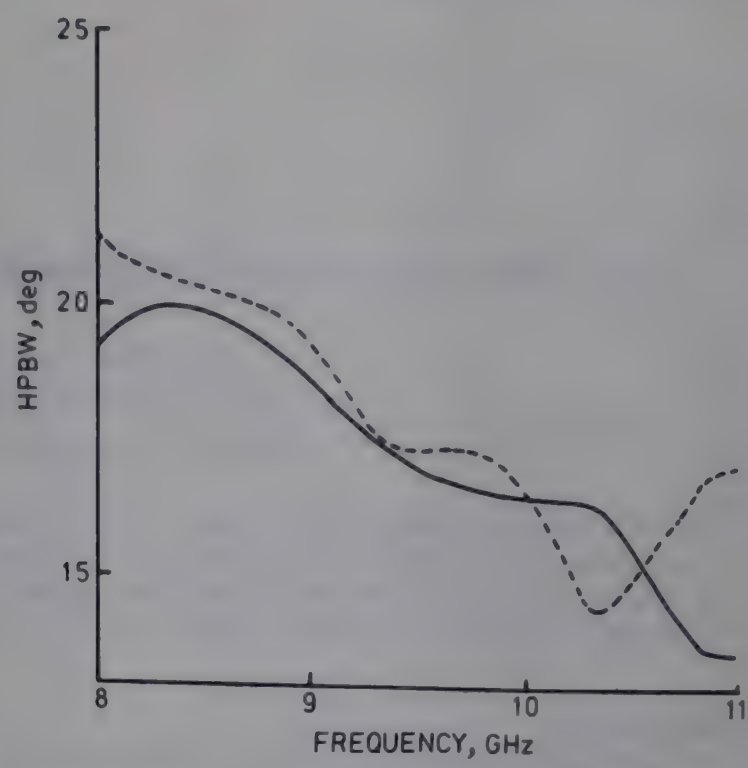

Fig. 7—Variation of HPBW with frequency when the flange is kept at the optimum position at $2\beta = 60°$ and $N=9$ (-----, *H*-plane; ——, *E*-plane)

symmetrical *E*- and *H*-plane patterns. Compared to a fixed compound horn[5], the present system offers great convenience in adjusting the antenna characteristics by trimming the flange parameters, i.e. by adjusting the flange position, we can obtain sharp, broad, or split beams.

Acknowledgement

One of the authors (CKA) gratefully acknowledges the financial assistance accorded by the Council of Scientific and Industrial Research, New Delhi. Thanks are also due to Prof. K Sathianandan, Head of the Department of Physics, University of Cochin, for providing laboratory facilities. The authors extend their thanks to Mr C B Muraleedharan for his valuable help in fabricating the antenna turn-table.

References

1 Zachariah E J, Vasudevan K & Nair K G, *IEEE Trans Antennas & Propag (USA)*, **27** (1979) 708.

2 Mohanan P, Pravinkumar P A & Nair K G, *Indian J Radio & Space Phys*, **11** (1982) 112.

3 Lawrie R E & Peters L, *IEEE Trans Antennas & Propag (USA)*, **14** (1965) 605.

4 Nair K G & Srivastava G P, *J Inst Electron & Telecommun Eng (India)*, **13** (1967) 76.

5 Chandra Mouly M C, *J Inst Electron & Telecommun Eng (India)*, **63** (1982) 81.

Indian Journal of Radio & Space Physics
Vol. 13, February 1984, pp. 16-18

Solar Wind Interaction Region & Low Latitude Geomagnetic Field

G K RANGARAJAN & R S RAMTEKE*
Indian Institute of Geomagnetism, Bombay 400005

Received 2 *February* 1983; *accepted* 21 *August* 1983

The influence of passage of solar wind interaction region where fast plasma overtakes the slow wind on low latitude geomagnetic field, is studied over a solar cycle. It is shown that the transit of interaction region is followed by significant geomagnetic changes. The magnitude of the change is a function of solar activity and local time. Solar wind velocity rather than the north-south component of IMF seems to be crucial parameter in the geoeffectiveness of the interaction region.

1 Introduction

It has been well established that interplanetary streams influence the geomagnetic field in several significant ways, the magnitude depending on the latitude and longitudinal sector of the place of observation. High speed solar wind streams have also been shown to influence the geomagnetic activity. Sawyer and Haurwitz[1] found that index A_p of magnetic activity was better organized with the passage of high speed streams when compared to solar magnetic sector boundary passage. In analyzing the causes for recurrent geomagnetic storms, Burlaga and Lepping[2] suggested that neither the solar wind stream alone nor only fluctuations in the north-south component (B_z) of IMF can cause a storm and that the important parameter was the electric field, $E = -V \times B_z$, in causing enhanced geomagnetic activity.

When streams from coronal holes move through the interplanetary medium, fast solar wind plasma overtakes the slow plasma creating an "Interaction region" wherein density and magnetic field are enhanced[3]. From Pioneer-10 IMF data, Rosenberg *et al.*[4] found that only in the interaction region the B_z component was relatively large. Very recently Rosenberg and Coleman[5] studied the solar-cycle dependent north-south field configurations in the interaction region and found that enhanced southward B_z would occur in the leading part and northward B_z would dominate in the trailing portion of the interaction region. This configuration reversed in phase near the beginning of 1970, as did the solar dipolar-related dominant polarity effect[6]. Their Table 3 (Ref.5) provides the dates of observed interaction region between 1965 and 1973, covering both solar minimum and maximum epochs. These dates were identified from data compilation of King[7].

Low latitude geomagnetic activity is influenced by the passage of sector boundary which is also a velocity discontinuity[8] and also by high speed solar wind streams[9]. It is, therefore, natural to identify the extent to which transition of solar wind interaction region influences the low latitude geomagnetic field. Recently, Bhatnagar *et al.*[10] have shown that about 65 % of solar interaction regions are associated with moderate to large changes in geomagnetic indices, A_p and K_p, and the balance, with quiet conditions of the geomagnetic field. In this paper we aim at finding the nature of the geomagnetic field change associated with the passage of the interaction region, both as a function of the time and the epoch of solar activity. The effects of B_z at equatorial latitudes on short-period oscillations are well studied[11] and the B_z control of substorm activity is quite well known. As the nature of the B_z component associated with solar interaction region has changed with time, we also aim at studying the corresponding change, if any, in the geomagnetic response.

2 Data

The mean hourly values of the horizontal intensity, H, derived from records and observations at Alibag (geogr. coord., 18°N, 73°E; dip 25°N), a low latitude station well away from the influence of auroral electrojet, are used in a superposed epoch analysis. Key days (zero epoch) are identified from the work of Rosenberg and Coleman[5] and the analysis is carried out to cover a span of 11 days (5 days on either side of the key day) separately for each UT hour and for each year.

3 Results and Discussion

The passage of solar wind interaction region is immediately followed by a drop in the field magnitude. The field level is usually at its highest on the day of the passage and maximum depression occurs on the next

*Present address: Central Water & Power Research Station, Pune 411024.

day or the following day. Some typical examples of the geomagnetic H response to passage of the interaction region are given in Fig.1. It is apparent that the magnitude of the depression is both a function of time and of solar activity. Comparison, for example, of the field changes on successive days centred on the key day for 0000 hrs UT of 1972 and 0600 hrs UT for 1973 highlight the differences.

We define a parameter, R, as the range of the field magnitude computed from the extreme values within the 11 days under consideration. Time progressions of R for each of the years considered for analysis are shown in Fig.2. The response, on the average, is higher during solar maximum years (1966-70) and lower close to solar minimum (1965). The main point of interest in these curves is the fact that the range R exhibits dominantly diurnal trend for certain years (1965 or 1969 for example) but is a composite of diurnal and semidiurnal modes for certain other years. Also, the amplitude of the diurnal oscillation changes with solar activity, largest amplitude being associated with the declining phase. The diurnal component, synthesized from the first harmonic for each year, is superposed on the actual variation curve in Fig.2 for visual comparison. In general, the peak magnitude is observed between 0900 and 1300 hrs UT, corresponding to the afternoon hours (1400 to 1800 hrs LT) in the Indian zone. As the low latitude field may be considered to be influenced mainly by the ring current intensity, it may be inferred that the larger response in the afternoon hours is indicative of the inflated evening sector in the ring current.

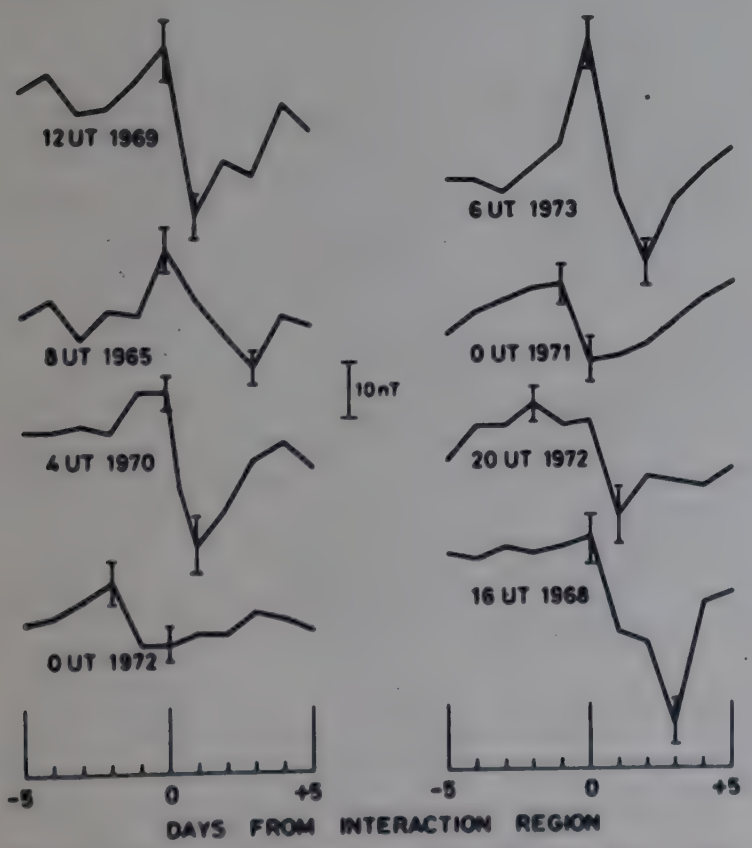

Fig. 1—Change in the geomagnetic horizontal field, H, for selected UT hours and years with the passage of solar interaction region (The vertical bars represent single standard error of the mean.)

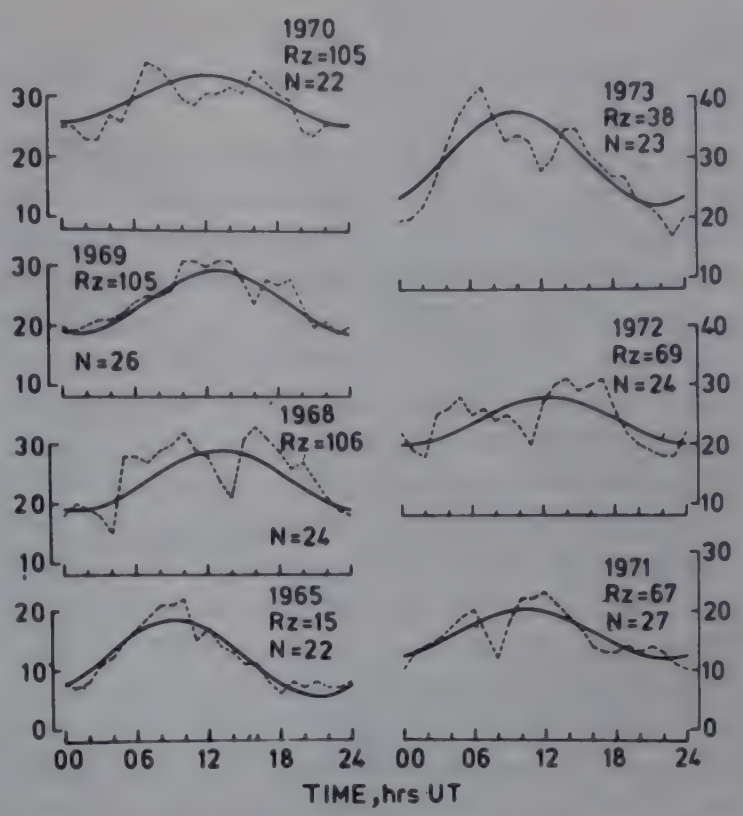

Fig. 2—Time variation of the response of the geomagnetic horizontal field, H, to the passage of solar interaction region for different years [Continuous line represents the first harmonic (diurnal component) of the data; R_z is the annual mean sunspot number and N is the number of key days.]

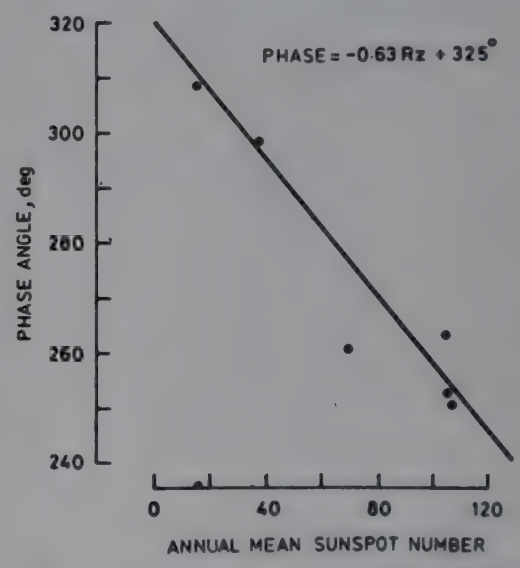

Fig. 3—Inverse relationship between the phase of the diurnal component and the annual mean sunspot number (The straight line is the best fit to the scatter plot in the least square sense.)

A close scrutiny of the phase of the diurnal component (i.e. epoch of maximum) for different years indicates an inverse relationship with solar activity as depicted by annual mean sunspot number. This feature is shown in Fig.3 where phase angle 0° corresponds to the peak at 0600 hrs UT and changes by 1 hr backward in time for each increase of 15°. Between sunspot numbers 0 and 100 (close to solar minimum and

average solar maximum) the phase change in the diurnal component is about 4 hr, the peak occurring later for more active periods.

The interaction region as deduced from the IMF data by Rosenberg and Coleman[5] (their Fig.1) has enhanced field magnitude and southward normal field component (B_N) in the initial part. However, according to them B_N was positive in the forward portion from 1964 up to 1969 and it reversed the phase near the beginning of 1970. The solar dipolar magnetic field polarity, which controls the dominant polarity effect of the interplanetary sector structure, was also known to be reversed following the solar maximum[12] in 1970.

Thus, if the southward component was the only controlling factor for enhanced geomagnetic activity, we can expect diminished response for the period 1964-69 as compared to the period 1970-73. While this may still be true in so far as magnetospheric substorms are concerned, it is not borne out from the present analysis for the low latitude geomagnetic field which is basically a measure of the ring current intensity. It, therefore, appears reasonable to conclude that the passage of the interaction region affects the low latitudes more through enhanced solar wind velocity than through the southward component of B_z. The fact that largest range of response was found during the declining phase of the solar cycle where high speed streams from coronal holes are more frequent, lends further support to this.

In conclusion we find that, similar to other solar related parameters like sector boundary and high speed streams, the solar wind interaction region also causes appreciable depression of the low latitude magnetic field and that the observed effect exhibits both local time and solar cycle dependence.

References

1 Sawyer C & Haurwitz M, *J Geophys Res (USA)*, **81** (1976) 2435.

2 Burlaga L F & Lepping R P, *Planet & Space Sci (GB)*, **25** (1977) 1154.

3 Smith E J & Wolfe J H, *Geophys Res Lett (USA)*, **3** (1976) 137.

4 Rosenberg R L, Kivelson M G & Coleman P J (Jr), *J Geophys Res (USA)*, **83** (1978) 4165.

5 Rosenberg R L & Coleman P J (Jr), *J Geophys Res (USA)*, **85** (1980) 3021.

6 Rosenberg R L & Coleman P J (Jr), *J Geophys Res (USA)*, **74** (1969) 5611.

7 King J H, *Interplanetary Magnetic Field Data Book, NASA-NSSDC TS-04*, 1975.

8 Rangarajan G K, *Planet & Space Sci (GB)*, **25** (1977) 465.

9 Rangarajan G K & Arora B R, *Indian J Radio & Space Phys*, **10** (1981) 54.

10 Bhatnagar V P, Jakobsson T & Rosenberg R L, *Planet & Space Sci (GB)*, **30** (1982) 1079.

11 Agarwal A K, Rastogi R G, Nityananda N & Singh B P, *Nature (GB)*, **273** (1978) 5653.

12 Wilcox J M & Scherrer P H, *J Geophys Res (USA)*, **77** (1972) 5385.

Indian Journal of Radio & Space Physics
Vol. 13, February 1984, pp. 19-23

Behaviour of Space Charge Before & After Rains at a Valley Station

V N REDDY MUKKU
Department of Physics, University of Roorkee, Roorkee 247 667
and
M K KHERA, A R RAFIQUE & P N RAINA
Department of Physics, University of Kashmir, Srinagar 190 006

Received 30 *April* 1983; *accepted* 18 *July* 1983

Space charge measured with passive antenna system shows slightly negative values during nighttime, but highly negative ones during daytime in the layer 1/2-1 m. Immediately after a heavy spell of rain the space charge in the same layer becomes positive in the daytime tending to become negative during nighttime. Long after the rains, the space charge retained the same behaviour as before rains. The various possibilities for the observed phenomenon have been discussed.

1 Introduction

Space charge density can be defined as the net charge in unit volume element. In fair weather, the space charge can be produced in several ways by natural and artificial sources. Vertical inhomogeneity of electrical conductivity, electrode effect, bubble breaking and surfing over oceans, voltaic charge transfer, electrochemical charge separation, carrying of space charge by air currents from the cloudy regions; etc. are the natural processes, and high tension cables, man-made pollution, etc. are the artificial processes, which can introduce the space charge into atmosphere. The distribution of space charge will be governed by the meteorological conditions. Predominantly, there are two types of diurnal variations in space charge, viz. (i) daytime high and nighttime low and (ii) daytime low and nighttime high space charges.

In strong turbulent conditions of convective mixing characterized by high winds and good visibility, Scrase[1] obtained positive space charge at all levels, with concentration increasing with height. Bent and Hutchinson[2] obtained a somewhat similar result by measuring space charge density at 1 and 19 m. In quiet and stagnant air Scrase[1] obtained negative space charge in the lowest level of 5 m and above that positive space charge.

Law[3] observed a good positive correlation between the lapse rate and space charge density (i.e. high during daytime and low at night) at Cambridge, England, somewhat similar to that of Moore *et al.*[4]

On the other hand, Sharpless *et al.*[5] and Aspinall[6] obtained daytime minimum and nighttime maximum in the space charge density measured at Lanehead.

In this paper we report and discuss the results of space charge measurements obtained before, immediately after and long after the occurrence of heavy rains at Kashmir University Campus.

2 Site and Measurement Technique

The measurements were made in a lawn behind the Physics Department of Kashmir University, Srinagar (34°05 N, 74°50 E). Srinagar is a valley station filled with much human activity compared to mountain station Gulmarg. The nearest pollution source is about 100 m away from the observatory. The period of smoke was not considered in the analysis.

The air-earth current was measured by an insulated aluminium plate kept at the ground level in a pit. The charge collected by this plate was fed to an electrometer amplifier through a high resistance of $10^{10}\Omega$. To account for displacement currents, Kasemir's[7] compensator, which gives a time constant of about 9 min, was used.

The space charge was measured by the procedure similar to Crozier[8] by using the passive antenna system described earlier by Khera and Raina[9]. Two passive antennas, one at 1-m level and the other at 1/2-m level, were installed; these antennas give the atmospheric potentials at their respective levels. Space charge was then derived from Poisson's equation.

3 Space Charge Before and Long After Rains

Fig.1 gives some examples of diurnal variation in space charge density at Kashmir University Campus. The wind speed is generally less than 1 m sec $^{-1}$. It is clear that space charge density in the layer between 1 m

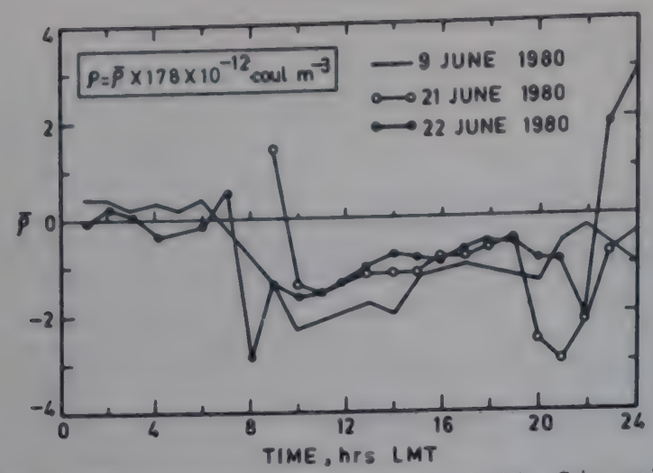

Fig. 1—Diurnal variation of space charge density ($\bar{\rho}$) at Srinagar in the layer between 1 and 1/2 m above the ground before rains

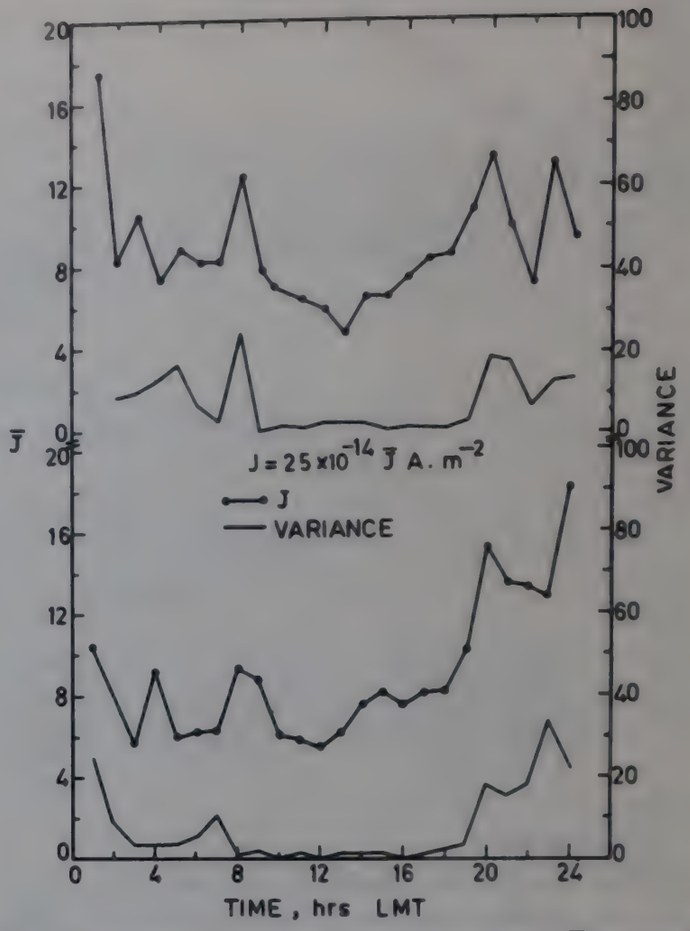

Fig. 2—Diurnal variation of air-earth current density ($\bar{J}$) measured at the ground level at Srinagar

and 1/2 m is highly negative in the daytime and somewhat less negative at night. There is, however, a tendency for it to become positive in the early morning hours. With dawn the space charge becomes negative which becomes afterwards less with dusk. This seems to be the usual feature of this station which is similar in many ways to that observed by Raina[10] at Gulmarg. Raina also measured the space charge density by the same procedure as we have used here.

In an attempt to see the contribution of convection current (mechanical transfer current) Aspinal[6] observed that this is of the same magnitude as the conduction current and almost entirely governs the diurnal variation of the total air-earth current. The total air-earth current at Lanehead is lower during the daytime than at night. Accordingly, the space charge measured at a height of 0.8 m also shows lower values during day (upward convective) than night.

The air-earth current density measured at our campus (Fig.2) also shows lower values during day than night. Moreover, the space charge is not only low but also it becomes negative with convection set-ups. The small values of air-earth current in the vertical convective period suggest the removal of small ions by the eddy diffusion forces. It is because of the fact that the velocity of small ions with mobility about 1.14×10^{-4} m^2 V^{-1} sec^{-1} under the electric field 100 V m^{-1} is 1.14×10^{-2} m sec^{-1}, which is at least ten times smaller than the vertical eddy diffusion forces.

We may explain the existence of negative space charge between 1 m and 1/2 m despite the formation of positive space charge due to electrode effect, by considering the conduction current at all levels to be the same. We have

$$\nabla . I = 0$$

$$\frac{\lambda \rho}{\epsilon_0} + E\frac{d\lambda}{dz} = 0$$

or

$$\rho(z) = -\epsilon_0 \frac{I}{\lambda^2}\frac{d\lambda}{dz} \qquad \ldots (1)$$

Eq.(1) indicates that space charge concentration is quite sensitive to the vertical distribution of conductivity in the atmosphere. Whenever a current is flowing, accumulation of space charge will occur at the boundaries of layers where the conductivity of air changes. For example, if there is a stratum of air having low conductivity, such as haze layer we would expect the accumulation of space charge at the top and bottom of the haze layer. If we consider a small volume element above the haze layer the number of positive ions which enter into it from its top will be more than those which leave from bottom. In this way positive ions would accumulate to form a layer of positive charge. At the bottom of haze layer upward moving negative ions would accumulate to form a layer of negative space charge. These considerations were confirmed in the aircraft survey of Moore *et al.*[4]

Applying the same logic we can explain the occurrence of negative space charge between 1 m and 1/2 m if there is intense ionization close to the ground. In the presence of such layer, the upward moving negative ions would accumulate to form negative space charge at the top boundaries of the layer of intense ionization. The downward moving positive ion would now accumulate at the bottom boundary of the layer of intense ionization to form positive space charge. The bottom boundary of the intense ionization in this

case will amost be the ground. Thus one can find a stratum of positive space charge close to the ground and negative space charge above it in the presence of intense ionization which is the case studied by Crozier[8] at a semi-desert site near Socorro. It should be noted that convection of positive space charge will not neutralize the negative space charge lying above it, because the number of positive ions convected upwards will be equal to the convected number of negative ions. Thus, stratification of space charge will continue as long as intense ionization occurs close to the ground. The space charge formation due to this kind of vertical inhomogeneity in the conductivity profile was named by Israel[11] as generalized electrode effect which should not be confused as normal electrode effect. It should be noted that normal electrode effect is believed to be masked by the generalized electrode effect.

Intense ionization close to the ground even in the presence of upward convection is believed to be due to the delay in the diffusion of exhaled radioactivity into atmosphere. The concentration of short-lived radioactivity decreases with height and the scale height of its profile will change with meteorological conditions[12–17].

It can be seen from Fig. 1 that after sunset the negative space charge becomes less and that it becomes slightly positive in the early morning hours. Working at low pollution conditions Raina[10] also noticed such a kind of behaviour at Gulmarg. He also observed positive space charge just above a height of 1/4 m during day and slightly negative during night. If it is true for Srinagar also, then one may have to think in terms of drastic changes in conductivity profile between day and night within 1-m level. However, no plausible explanation can be offered to explain early morning positive space charge between 1 m and 1/2 m.

4 Space Charge Immediately After Rains

Srinagar experienced heavy spells of rain during June and the first week of July 1980. The measurements of atmospheric electric parameters were resumed about one day after the rains. During these observations, we have measured the wind speed with Rose anemometer whenever we felt the wind. These measurements revealed that the winds are generally quite low (usually less than 1 m sec^{-1}) at this station. Whenever there is smoke from a hut (which is about 100 m away from the observatory), it was considered as disturbed and was not considered in the analysis of electric elements. The cloudy conditions were noted according to the changes that occurred in the sky. For example, the duration of the continued envelope of a cumulus cloud and the transformation of one form of cloud to another, and also their movements were noted. Mostly clouds observed during this period were of low level ones such as Ac, As, C, Cs, Cn, etc. We have noticed the occurrence of lightning flashes late in the evening at distances far away from the station. But on several occasions the excursion of thunderclouds close to the observatory was observed. These thunderclouds used to dissipate after presentation of lightning and raingush while pasing through observatory. Such periods were also omitted from our analysis. Fig.3 shows the behaviour of space charge density for 7 and 8 Aug.1980 in the layer between heights of 1 and 1/2 m from the ground.

It can be seen that space charge becomes positive, 4 to 5 hr after sunrise. It reaches a maximum value at 1700 or 1800 hrs LMT and drops afterwards. This behaviour was also noticed on 10,11,12 and 13 Aug.1980 (not shown here). Fig.4 gives the behaviour of space charge for the period of 19-22 Aug.1980. On

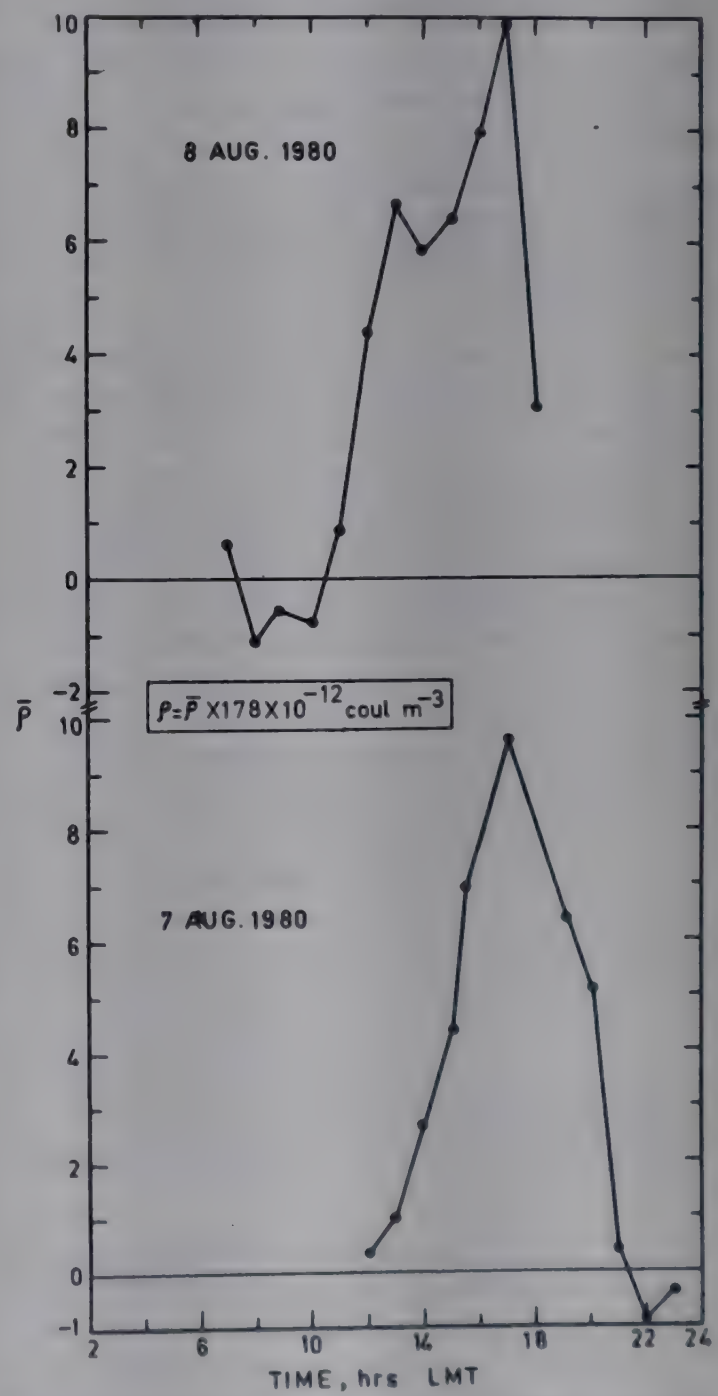

Fig. 3—Variation of space charge density at Srinagar in the layer between 1 and 1/2 m above the ground one day after heavy rains

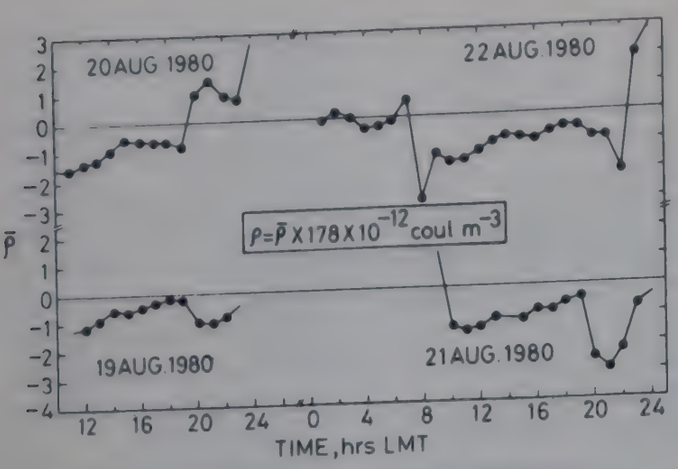

Fig. 4—Same as Fig.3 but 12 days after rains

these 4 days the cloudy content was reduced. But the cloudiness continued over surrounding mountains. Also, distant lightning flashes which were observed earlier (corresponding to Fig.3) were not observed.

It can be seen that the space charge is positive immediately after rains (Fig.3) than before rains. Afterwards it again attained negative values. Another interesting feature is that the space charge density recorded by us and Khera and Raina[18] immediately after the rains is much greater in magnitude than that of negative space density recorded before and long after the rains.

The average value of space charge density in the layer between the heights of 1 and 1/2 m above the ground for the period 1200-1700 hrs LMT is about 9×10^{-10} coul. m^{-3} which corresponds to about 5×10^9 elementary charges (el.) per m^3. Khera and Raina[18] attributed this to the normal electrode effect which occurs in the absence of inhomogeneity near the ground level. Conductivity inhomogeneity may be caused by intense ionization or drastic changes in aerosol concentration. They explained that as the water seeps into considerable depths a reduction in the flux of radon-222 and radon-220 (thoron) can occur because of filling of soil capillaries and interstices. This reduction in ionization rate will allow the normal electrode effect to predominate at the ground level. Khera and Raina[18] further obtained a reduction in the positive space charge density as time passes. They explained it in terms of the gradual decrease in moisture content of the ground as the water evaporates into the atmosphere with lapse of time and the consequent gradual increase in radioactive flux from the ground.

From Table 1 of the work of Israel[19] it is clear that the space charge density that can be possible due to normal electrode effect is 2×10^{-10} to 4×10^{-10}coul. m^{-3}. Muhleisen[20] obtained a mean space charge density of 1.6×10^{-10}coul. m^{-3} whereas average space charge density observed for the period 1200-1700 hrs LMT is about 9×10^{-10}coul.m^{-3}. The highest value obtained is about 22×10^{-10}coul.m^{-3} which is about 4 times greater than the highest value predicted by the theories on normal electrode effect. And because of this reason perhaps, Crozier[5,11,21] explained the existence of high positive space charge density close to the ground and negative space charge above it on low-windy nights in terms of enhanced ionization due to the accumulation of radon and thoron close to the ground due to temperature inversion. The average of space charge densities for the period 1200-1700 hrs LMT before and about 12 days after the rains is about -1.5×10^{-10} coul. m^{-3}. This corresponds to about 10^9 el. m^{-3}. If normal electrode effect can account for the observed behaviour immediately after rains then on normal days there must be an ionization rate which can give an equilibrium small ion concentration of about $(5 \times 10^9 + 1 \times 10^9)$ el. m^{-3} near the ground level so that normal electrode effect can be masked by this intense ionization.

Another feature we should see is the behaviour of space charge density before and long after the rains in the nighttime. Before and long after the rains, the space charge density tends to become positive in the night compared to daytime. If daytime space charge density observed immediately after the rains is due to the reduction in the radioactive flux, then the positive space charge density should further increase in the night because of the reduced convection. But, not only our observations but also the observations of Khera and Raina[18] show a tendency towards negative values in the night. From all these considerations it seems that the high positive space charge that appeared near the ground level may not be totally due to the normal electrode effect.

We also attempted to see any possible influence of change in mixing height on space charge density at the ground level, because any reduction in the mixing height immediately after the rains can increase the particulate content in the mixing layer which in turn leads to the formation of space charge in the mixing layer. The mixing height can be calculated by extending a dry adiabate from the surface temperature to its intersection with the undisturbed temperature profile of that day similar to that in the work of Holzworth[22]. By undisturbed profile, it is meant that the profile is unaffected by the daytime heating of the ground and air. With the help of radiosonde data collected by India Meteorological Department at Srinagar we have calculated the mixing height for before, immediately after and long after the rains. These calculations revealed no apparent correlation between space charge density at the ground level and mixing height.

In addition to the normal electrode effect, the deposition of space charge brought by the air currents from cloudy area similar to that in the study by Imayanitov and Chubarina[23] may contribute to the observed behaviour. The clouds were existing mostly in daytime over nearby mountains and other places. In the night, as these clouds dissipate with lightning discharges, the space charge at our station attains a value which should be when there is reduction in radioactive flux (that is little negative or positive). Long after the rains the absence of nighttime lightning and presence of daytime negative space charge support this view. Since the clouds are distant and the order of electric field before and after the rains is almost the same, the effect of electric field on space charge can be ruled out.

Another possibility could be reduction in the intensity of convection. When there is reduction in convection, then the giant nuclei lifted from soil may be trapped in the layer close to the ground. This can again cause increase in the space charge close to the ground.

It should be noted that if the electrical conductivity at any station is predominantly determined by radioactivity, then the above observed effects will become predominant. If aerosol concentration is the determining factor (for example, in highly polluted cities) then the situation will be different. Washing out of aerosol particles by heavy rains can increase conductivity in the layer close to the ground compared to a normal day. This would lead to negative space charge immediately after heavy rains which is the case observed at Durham by Smiddy and Chalmers[24].

More measurements with better equipment at some other places will be helpful in recognizing the process responsible for this phenomenon.

Acknowledgement

The authors appreciate the stimulating discussions with Prof. N C Varshneya. They also acknowledge the financial support from University Grants Commission, New Delhi.

References

1 Scrase F J, *Meteorological Office Geophysics Memoirs, No.* **67**, HMSO, London, 1935.

2 Bent R B & Hutchinson W C A, *J Atmos & Terr Phys (GB)*, **28** (1966) 53.

3 Law J, *Q J R Meteorol Soc (GB)*, **89** (1963) 107.

4 Moore C B, Vonnegut B, Semonin R G, Bullock J W & Bradley W, *J Geophys Res (USA)*, **67** (1962) 1061.

5 Sharpless G T, Aspinall W P & Hutchinson W C A, *J Geomagn & Geoelectr (Japan)* **23** (1971) 335.

6 Aspinall W P, *J Geophys Res (USA)*, **77** (1972) 3196.

7 Kasemir H W, *Geophysics research paper No.* **42** in *Proceedings of the conference on atmospheric electricity*, edited by R E Holzer and W S Smith (Air Force Cambridge Research Center, U S Department of Commerce, Washington DC), 1955.

8 Crozier W D, *J Geophys Res (USA)*, **70** (1965) 2785.

9 Khera M K & Raina B N, *Indian J Meteorol Hydrol & Geophys*, 23 (1972) 543.

10 Raina B N, *Studies in atmospheric electric elements*, Ph D thesis, University of Kashmir, Srinagar, 1976.

11 Israel H, *Atmospheric electricity, Vol.* 2 (Isreael program for scientific translations, Jerusalem), 1973.

12 Crozier W D & Biles N B, *J Geophys Res (USA)*, **77** (1966) 4735.

13 Crozier W D, *J Geophys Res (USA)*, **74** (1969) 4199.

14 Hosler G R, *J Geophys Res (USA)*, **47** (1969) 7018.

15 Ikbe Y, *J Met Soc Jpn (Japan)*, **48** (1970) 461.

16 Ikbe Y & Shimo M, *Tellus (Sweden)*, **24** (1972) 29.

17 Beck H L, *J Geophys Res (USA)*, **29** (1974) 2215.

18 Khera M K & Raina B N, *J Atmos & Terr Phys (GB)*, **40** (1978) 1297.

19 Israel H, *Atmospheric electricity, Vol.*1 (Israel program for scientific translations, Jerusalem), 1971, 35.

20 Muhleisen R, *J Atmos & Terr Phys (GB)*, **20** (1961) 74.

21 Crozier W D, *J Geophys Res (USA)*, **68** (1963) 3451.

22 Holzworth G C, *J Appl Meteorol (USA)*, **1** (1962) 366.

23 Imyanitov I M & Chubarina E V, *Electricity of the free atmosphere* (Israel program for scientific translations, Jerusalem), 1967.

24 Smiddy M & Chalmers J A, *Q J R Meteorol Soc (GB)*, **85** (1960) 237.

Indian Journal of Radio & Space Physics
Vol. 13, February 1984, pp. 24-28

Fair Weather Atmospheric Electric Variability

V N REDDY MUKKU & N C VARSHNEYA
Department of Physics, University of Roorkee, Roorkee 247 667
and
M K KHERA
Department of Physics, University of Kashmir, Srinagar 190 006

Received 13 *May* 1983

An attempt is being made to explain the transition of atmospheric ohmic law parameters from one course to another course of variation. A comparison with the annual variation of these parameters at a land station and their behaviour during onset and dissipation of fog shows that the explanation is closely reasonable within the context of assumptions we have made. On the same theoretical basis, if conductivity in the upper atmospheric layers increases during sunrise and decreases during solar eclipse, the behaviour of other two ohmic parameters can be explained.

1 Introduction

At a land station the ground-based measurements of Ohm's law parameters in fair weather show a deviation from oceanic and polar continental station values. This has been attributed to the meteorological influences on atmospheric electric parameters. Quite often we come across some complex variations in these parameters; for example, the three parameters go in same phase, one goes opposite to the other two, etc. In this paper we have attempted to give some explanation for the transition from the usual course to another course of variation.

2 Theory

Fig. 1 shows a simplified atmospheric electric circuit. Since the meteorological variations in the upper atmosphere differ from that of ground level, the variations in R_a must also differ from that of R_g. Thus, if we assume that the potential difference between electrosphere and earth is constant for a short interval, then the potential drop between R_a and R_g will depend on their variations induced by the meteorological factors in that short interval.

This implies, that even if R_g and R_a are constant with time, the variations in R_a can cause the variation in conduction current and hence the potential drop across R_g. We shall treat the quantity R_g in a somewhat simple manner because one does not exactly know the nature of correlation between synoptic meteorological conditions and R_g. From the compilation of experimental data an empirical formula for the altitude variation of small ion density was given by Barr[1] as

$$n(z) = n_f - (n_f - n_g)e^{-pz} \quad \ldots (1)$$

where n_g is the concentration of small ions at the ground level, n_f is a constant and $1/p$ is scale height. An approximate equation for equilibrium concentration of small ions is quoted well in the literature. This depends on the ionization rate and aerosol particle distribution which, in turn, depends on the meteorological conditions.

In atmosphere, since the density of gas decreases exponentially with the altitude we can write for mobility (k)

$$k(z) = k_g\, e^{-sz} \quad \ldots (2)$$

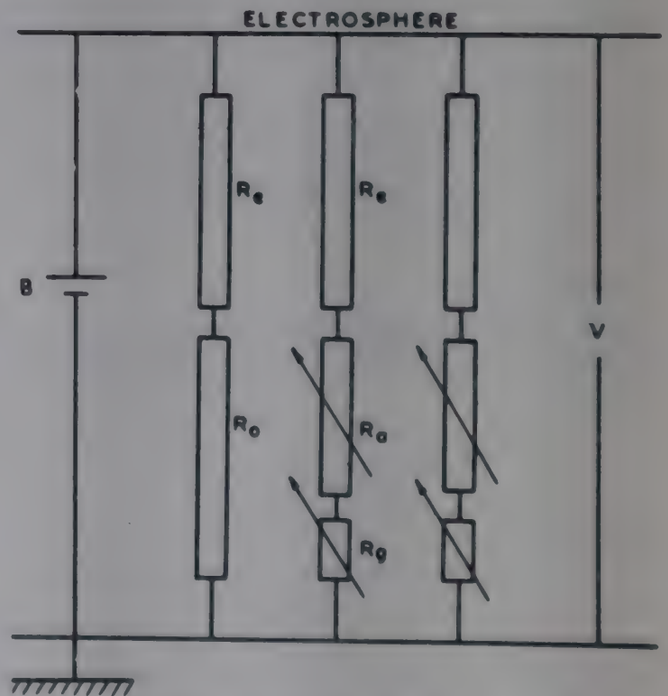

Fig. 1—A simplified atmospheric electric circuit [B, battery (probably thunderstorm): $R_g = \alpha\lambda_g$, variable resistance in the exchange layer, in which atmospheric electric measurements are usually made and α is the proportionality factor; R_a, variable resistance in the troposphere; $R_a + R_e = R_c = \frac{1}{\beta\lambda_c}$, resistance above the exchange layer; and $(R_0 + R_e)$, oceanic columnar resistance]

Making a crude assumption that $p=s$, and combining Eqs. (1) and (2) we obtain for conductivity

$$\lambda(z)=\frac{\lambda_g}{1-A}\,(1-A\,e^{-pz})\,e^{pz} \qquad \ldots (3)$$

where

$$A=1-\frac{n_g}{n_f} \qquad \ldots (4)$$

and

$$\lambda_g=n_g\,k_g\,e$$

The altitude variation of resistivity (γ) is given by

$$\gamma(z)=\frac{(1-A)\,e^{-pz}}{\lambda_g\,(1-Ae^{-pz})} \qquad \ldots (5)$$

This can be expanded to give the form

$$\gamma(z)=\left(\frac{1-A}{\lambda_g}\right)(e^{-pz}+Ae^{-2pz}+A^2e^{-3pz}+\ \ldots) \qquad \ldots (6)$$

It is noteworthy that Gish[2] gave formula, based on the compilation of experimental data for the resistivity and his formula contains three exponential terms quite similar to those in Eq. (16) if truncated after 3 terms.

The resistance in a column of atmosphere from the surface of earth to an altitude z is given by

$$R(z)=\int_0^z\frac{dz}{\lambda(z)}$$

$$=\left(\frac{1-A}{pA\ \lambda_g}\right)\ln\left(\frac{1-A\,e^{-pz}}{1-A}\right) \qquad \ldots (7)$$

Therefore, the columnar resistance R is given by

$$R_g+R_a+R_e=\left(\frac{1-A}{pA\ \lambda_g}\right)\ln\left(\frac{1}{1-A}\right) \qquad \ldots (8)$$

The columnar resistance R_g within the exchange layer is given by

$$R_g=\left(\frac{1-A}{pA\ \lambda_g}\right)\ln\left(\frac{1-A\,e^{-pH}}{1-A}\right)$$

$$=\frac{1}{\alpha\lambda_g} \qquad \ldots (9)$$

where $\alpha=\dfrac{pA}{(1-A)\ln\left(\dfrac{1-Ae^{-pH}}{1-A}\right)}$

and H is the height of exchange layer.

For brevity, let us put $(R_a+R_e)=R_c=1/\beta\lambda_c$ where β is proportionality constant and variations in R_c can be understood as only due to the R_a. We assume that the convection currents and local space charge influences on electric field are absent during the period of transition so that the Ohm's law is valid. Therefore,

$$V=I\,\frac{\alpha\lambda_g+\beta\lambda_c}{\alpha\lambda_g\cdot\beta\lambda_c} \qquad \ldots (10)$$

If V is constant for a short period during which we observe transition from one state to another state of variation, then we can classify some of the possible modes of variations in the following way.

CASE I: $\beta\lambda_c/\alpha\lambda_g$ is constant

(i) By increasing the values of $\beta\lambda_c$ and $\alpha\lambda_g$

When $\beta\lambda_c$ and $\alpha\lambda_g$ increase suddenly by maintaining their ratio constant, we find at the ground

Increase in $\alpha\lambda_g$
Increment in I
Constancy in E

(ii) By decreasing the values of $\beta\lambda_c$ and $\alpha\lambda_g$

Decrement in $\alpha\lambda_g$
Decrement in I
Constancy in E

The meaning of Case I is that the electric field at the ground level need not necessarily change for every change in conductivity at the ground level. The columnar resistance can be written from Eq. (8) as

$$R=1/\gamma\lambda_g$$

where $\gamma=\dfrac{pA}{(1-A)\ln\left(\dfrac{1}{1-A}\right)}$

Eq. (10) then becomes

$$V=IR \qquad \ldots (11)$$

or

$$R=\gamma V \qquad \ldots (12)$$

for $E\,\lambda_g=I$ $\qquad \ldots (13)$

If γ remains constant during the course of the day we can derive from Eq. (12)

$$\frac{1}{E}\frac{dE}{dt}=\frac{1}{V}\frac{dV}{dt}$$

This implies that if γ remains constant with time then electric field at the ground level will show the same percentage of variation as ionospheric potential does irrespective of what is happening with current and conductivity at the ground level. Another conclusion we can derive from Eq. (11) is that if R remains constant with time, then I will go in phase with V irrespective of what is happening with the other parameters. If γ as well as λ_g remains constant with time, then we can derive from Eqs. (12) and (13)

$$\frac{1}{E}\frac{dE}{dt}=\frac{1}{V}\frac{dV}{dt}=\frac{1}{I}\frac{dI}{dt}$$

This shows that not only the parameters A and p which determine the vertical distribution of resistivity but also the magnitude of resistivity should remain constant with time to keep the conduction current and potential gradient in phase with ionospheric potential. Over oceans, polar regions and high mountain stations

particularly in winter[3] the magnitude of columnar resistance and its vertical distribution remain constant during the course of the day. Thus, we get E and I in phase with V. Since there is no solar particle penetration during the solar flares at low latitudes, the screening of galactic cosmic rays will cause reduction in the conductivity throughout the column between ionosphere and the ground[4]. Since the reduction in conductivity occurs throughout the column, the parameters involved in conductivity scale height will not undergo change but the columnar resistance will increase. Thus during solar flares, the electric field over low latitude oceanic and high mountain stations would go in phase with ionospheric potential as usual. But the course of conduction current would deviate from ionospheric potential mode.

The study of relationship between the parameters involved in the conductivity scale height and synoptic meteorological conditions is very important in the mapping of electric field and separation of local and global influences. Scarcity of data on this topic rather limits our discussion.

CASE II: $\beta\lambda_c/\alpha\lambda_g$ is increasing

(i) By decreasing $\alpha\lambda_g$ and keeping $\beta\lambda_c$ constant
Decrement in $\alpha\lambda_g$
Decrement in I
Increment in E

(ii) By keeping $\alpha\lambda_g$ constant and increasing $\beta\lambda_c$
Constancy in $\alpha\lambda_g$
Increment in I
Increment in E

(iii) By increasing $\alpha\lambda_g$ and increasing $\beta\lambda_c$ more than $\alpha\lambda_g$
Increment in $\alpha\lambda_g$
Increment in I
Increment in E

CASE III: $\beta\lambda_c/\alpha\lambda_g$ is decreasing

(i) By increasing $\alpha\lambda_g$ and keeping $\beta\lambda_c$ constant
Increment in $\alpha\lambda_g$
Increment in I
Decrement in E

(ii) By keeping $\alpha\lambda_g$ constant and $\beta\lambda_c$ decreasing
Constancy in $\alpha\lambda_g$
Decrement in I
Decrement in E

Some other cases are also possible. We may now compare some of the above cases with some established experimental results.

3 Annual Variation in Ohmic Law Parameters

Fischer and Muhleisen[5] studied the ionospheric potential variations during the period (1959-71) by balloon radiosonde ascents at Weissenau (South-West Germany) and found no significant seasonal variation. Uchikawa[6] found 18% amplitude of the mean value for the annual mode at Weissenau (see Muhleisen's comment in the discussion part of Uchikawa's paper). However, Uchikawa[6] found no significant seasonal variation in ionospheric potential measured at Syowa-Base. Accordingly, the potential gradient over oceans show no significant seasonal variation[7]. From these results we may assume no seasonal variation in ionospheric potential. On the other hand conductivity and conduction current decrease and potential gradient increases in winter compared to summer at most stations of the world.* We may verify this feature from Case II(i). Since the winter value of $R_g = 1/\alpha\lambda_g$ is greater than the summer value with $(R_e + R_a)$ remaining constant, the ratio $\beta\lambda_c/\alpha\lambda_g$ will increase in winter compared to summer. Hence I decreases and R increases in winter compared to summer.

Over the clean areas nearly 45% of columnar resistance will come from the exchange layers. Over the polluted areas 70-90% of columnar resistance will come from the exchange layer[9-11]. This is the only suitable information which we can use in the estimations of parameters A and p. Since the vertical distribution of conductivity above the exchange layer is dependent on the galactic cosmic rays, we can assume it to be almost the same for every station. Then as the amount of pollution and height of exchange layer change, the percentage of resistance in the exchange layer and the values of A and p will change. For relatively clean areas we may take for summer $\lambda_g = 2 \times 10^{-14}\,\Omega^{-1}\,m^{-1}$ and $R \simeq 1.13 \times 10^{17}\,\Omega m^2$. To achieve 45% of R (i.e. $R_g = 5.0 \times 10^{16}\ \Omega\,m^2$) in the exchange layer of height 2 km, we should take $A = 0.9$ and $p = 1.13 \times 10^{-4}\ m^{-1}$.

If the conductivity at the ground level is reduced by (say) 50% in winter, we may take $\lambda_g = 1.0 \times 10^{-14}\ \Omega^{-1}\ m^{-1}$ and $R = 1.5 \times 10^{17}\ \Omega\,m^2$. For $H = 2$ km, if we take $A = 0.3$ and $p = 5 \times 10^{-4}\ m^{-1}$, then the resistance in the exchange layer will be about 68% of R.

If we take $V = 240$ kV as suggested by Markson[10] then we get at the ground level in summer,

$I \simeq 2.1 \times 10^{-12}\ A\ m^{-2}$

and

$E \simeq 106\ V\ m^{-1}$

For the same value of V, we get at the ground level in winter

$I \simeq 1.6 \times 10^{12}\ A\ m^{-2}$

$E \simeq 160\ V\ m^{-1}$

*However, occasionally it can also occur the opposite way[8,9].

This shows that since R_c remains constant throughout the year, increase in the pollution will increase the total columnar resistance and percentrage of R_g in R. This would cause change in the values of A and p which in turn would lead to the change in the map of electric fields in the atmosphere.

4 Sunrise Effect

The decrement in conductivity and increment in conduction current and potential gradient is the general feature at the time of sunrise[9,12-15]. If the value of $\alpha\lambda_g$ decreases or remains constant, the increase in the value of $\beta\lambda_c$ can account for the above result (Case II). Even if there is no change in the R_g, any change in R_c induced by the sunrise will change the values of A and p and hence the percentage of resistance in the exchange layer.

Summarizing the results obtained up to 1967, Chalmers[8] states that the effect is more pronounced in summer compared to winter. The report of Mary Selvam *et al.*[15] indicates the suppression of sunrise effect with increasing pollution. For clean areas in summer, let us take the values of λ_g, A, p, H and V given earlier which give $I = 2.1 \times 10^{-12}$ $A\ m^{-2}$ and $E = 106$ $V\ m^{-1}$. At the time of sunrise even if there is no change in the conductivity at the ground level, a reduction in R_c by 20% would cause an increase of about 14% in the conduction current and potential gradient at the ground level.

For winter, taking the earlier given values of λ_g A, p, H and V which give $I = 1.6 \times 10^{-12}$ $A\ m^{-2}$ and $E = 160$ $V\ m^{-1}$, we get about 6% increase in E and I for the reduction of 20% in R_c. This indicates that as the amount of pollution increases in the exchange layer, the effect of sunrise on atmospheric electric elements will be suppressed.

5 Solar Eclipse Effect

Some of the reports on solar eclipse observations suggest increase in conductivity and decrease in potential gradient and conduction current[8,16-18].

Koenigsfeld[19] suggests that the variations observed in ground level atmospheric electric elements during solar eclipse should not only be seen in terms of meteorological influences in the exchange layer but also the variations in the amount and height of ozone and ionization of ice crystals by ultraviolet radiation. Studies of Devanarayanan and Mohan Kumar[20] indicate an increase of 50% in the partial pressure of ozone in the stratosphere. Even a 20% reduction in $\beta\lambda_c$ by any means over clean areas can account for the behaviour of E and I at the ground level (Case III). This also implies that the electric field aloft (may be above the exchange layer) should increase during the solar eclipse. Fig. 2 taken from Markson and Kamra[21]

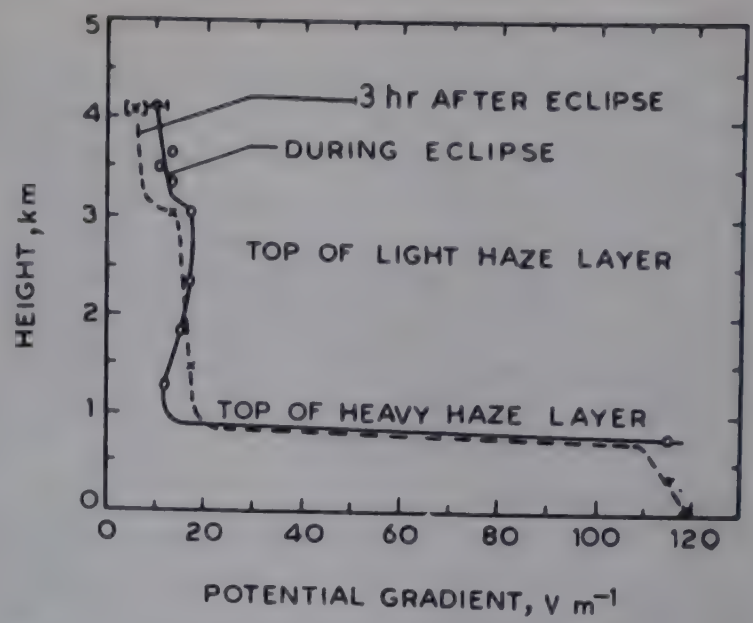

Fig. 2—Variation of atmospheric electric field with height during (solid line) and 3 hr after (broken line) eclipse[21]

supports our explanation. Markson and Karma[21] made aircraft investigation of electric field for the total solar eclipse of 7 Mar. 1970 at Norfolk, Virginia. The solid line represents the potential gradient during the partial phase of the eclipse following totality and dashed line indicates the same parameter about 3 hr after eclipse.

The former sounding during the partial phase of eclipse indicates increase of potential gradient about the mixing layer between 3 and 4 km and reduction between 1 and 2 km compared to the later sounding. They also noticed reduction in potential gradient at the ground level measurements for the same eclipse. This supports (Case III) the idea, of reduction in $\beta\lambda_c$. However, the effect of reduction in $\beta\lambda_c$ may not reflect in the ground based measurements at polluted areas. We are also aware of negative electric fields observed in the ground level measurements at some places[19,22] which can be explained by considering the formation of negative space charge due to the intense ionization caused by the trapping of radioactivity under the temperature inversion conditions similar to Crozier[23]

6 Fog Effect

The measurements during a widespread fog show a considerable increase in potential gradient, decrease in conductivity and slight decrease in conduction current compared to their fair weather value[3,8,9,24]. If $\alpha\lambda_g$ decreases during fog, and if we assume no change in $\beta\lambda_c$ then the ratio $\beta\lambda_c/\alpha\lambda_g$ will increase. The result can be understood from Case II(i). When the station gets out of the fog, the potential gradient decreases and conduction current and conductivity increase. This can be realized from the Case III(i). The negative electric fields and currents observed during intense fog can be explained by considering the sedimentation of negative charge carriers.

7 Conclusion

The variations in potential gradient and conduction current should be seen not only from conductivity variations at the ground level but also from the upper atmospheric layers. The simultaneous measurements of meteorological and electrical parameters at different altitudes of a station may help us in the separation of global and local influences on electric field. And also the formation of a network of such stations may help us in building a realistic mathematical model of atmospheric electric phenomena.

Acknowledgement

The authors wish to thank the University Grants Commission, New Delhi, for their financial support to this work.

References

1 Barr W C, *Atmospheric electric properties, United States Army Electronics Command, Fort, Monmouth, New Jersey*, 1969.
2 Gish O H, *Terr Magn Atmos & Electr (USA)*, **49** (1944) 159.
3 Reiter R, *Air Research and Development Command, US Air Force Contract No. AF* 61(052)-55, *Vol.* 1, 1960, 173.
4 Herman J R & Goldberg, *Sun, weather and climate* (NASA, Washington), 1978.
5 Fischer H J & Muhleisen R, *Meteorol Rundsch (Germany)*, **25** (1972) 6.
6 Uchikawa K, *Electrical processes in atmospheres*, edited by H Dolezalek & R Reiter (Dietrich Steinkopff, Darmastadt, West Germany), 1977, 460.
7 Mauchly S J, *Terr Magn & Atmos Electr (USA)*, **28** (1923) 61.
8 Chalmers J A, *Atmospheric electricity* (Pergamon, New York) 1967.
9 Isarel H, *Atmospheric electricity, Vol.* 2 (Israel Program for Scientific Translations, Jerusalem) 1973.
10 Markson R, *J Geophys Res (USA)*, **81** (1976) 1980.
11 Clark J F, *Recent advances in atmospheric electricity*, edited by L G Smith (Pergamon, New York) 1958, 61.
12 Ogawa T, *J Geomagn & Geoelectr (Japan)*, **12** (1960) 1.
13 Law J, *Q J R Meteorol Soc (GB)*, **89** (1963) 107.
14 Raina B N & Makhdomi B A, *J Atmos & Terr Phys (GB)*, **42** (1979) 155.
15 Mary Selvam A, Manohar G K, Khandelgaonkar S S, Rama Chandra Murty A S & Ramana Murty V, *Tellus (Sweden)*, **32** (1980) 232.
16 Bauer L A, Fisk H W & Mauchly S J, *Terr Magn & Atmos Electr (USA)*, **24** (1919) 1;87.
17 Mauchly S J & Thomson A, *Terr Magn & Atmos Electr (USA)*, **25** (1920) 41.
18 Israel H & Fries, *Z Geophys (Germany)*, **20** (1955) 137.
19 Koenigsfeld L, *Thunderstorm electricity*, edited by H R Byers (The University of Chicago, Chicago) 1963, 24.
20 Devanarayana S & Mohan Kumar K, *Proceedings of the international symposium on solar eclipse (Abstracts)*, edited by H Y Mohan Ram & S K Trehan (Indian National Science Academy, New Delhi) 1981.
21 Markson R & Kamra A K, *J Atmos & Terr Phys (GB)*, **33** (1971) 1107.
22 Kamra A K & Varshneya N C, *J Atmos & Terr Phys (GB)*, **29** (1969) 327.
23 Crozier W D, *J Geophys Res (USA)*, **70** (1965) 2785.
24 Dolezalek H, *Rev Geophys Space Phys (USA)*, **1** (1963) 231.

Communications

Indian Journal of Radio & Space Physics
Vol. 13, February 1984, pp. 29-31

Design, Development & Performance Evaluation of an Anechoic Chamber for Microwave Antenna Studies

E J ZACHARIAH*, K VASUDEVAN, P A PRAVINKUMAR, P MOHANAN & K G NAIR

Department of Electronics, University of Cochin, Cochin 682022

Received 7 *December* 1982; *revised received* 16 *May* 1983

The design, erection and evaluation procedures for a microwave anechoic chamber completed at Cochin University for antenna studies are presented. The chamber has an average reflectivity level of −32 dB at X-band frequencies, and it is comparable to international standards.

Antenna measurements and electromagnetic compatibility measurements require an environment free from external radio signal interference. Outdoor sites usually cause interference due to reflections from nearby objects and ground. Hence specially prepared indoor test ranges called anechoic chambers are used for conducting these experiments. An anechoic chamber is an artificially simulated free space environment in which RF propagation studies can be performed without any interaction from external sources. The design, development, and evaluation of a microwave anechoic chamber, recently completed in the Microwave Laboratory of the Cochin University, are described in this communication.

Microwave absorbing material is used to absorb electromagnetic energy in this frequency band. In the anechoic chamber described here, the absorber used is a polyurethane-foam-based one, with some microwave absorbing material dispersed inside. The material was cut into pyramidal or wedge shapes. The following types of material were employed in different portions of the chamber.

(i) Small pyramids of base 7.6 cm and height 15.2 cm were used on the ceiling, side walls, a major portion of the back wall, and a portion of the floor.

(ii) Larger pyramids of base 15.2 cm and height 45.7 cm were used on the central portion of the back wall from where reflections are most likely to occur.

(iii) Wedges of base width 10.2 cm and height 5.1 cm were used to cover the less important portions of the chamber, like the surfaces of the tapered section.

(iv) A layered flat sheet absorber having five layers and a total thickness of 15.2 cm was used on the walkways.

(v) A densely packed flat absorber of thickness 5.1 cm had been put beneath all of the above mentioned types to increase the total absorption.

Before stacking these material inside the chamber, their reflectivity was measured using the Arch[1] method. The small pyramids, with a 5.1 cm flat absorber at the back and a metallic sheet behind it, had a reflectivity of −35 dB. The wedge absorber had a slightly higher reflectivity. These values were considered adequate for the present application.

While taking the antenna measurements, the test antenna should be illuminated by a plane wave front[2]. For this, the minimum separation between the transmitting and the test antenna is $R = 2D^2/\lambda$ where R is the separation between the antennas, D the aperture diameter of the test antenna, and λ the operating wavelength. The length of the chamber should be more than this, since the test antenna has to be put in the quiet-zone, which occurs at some distance from the chamber walls also. The length of this chamber was chosen to be 7.2 m. Hence the chamber has an effective propagation length of about 6 m. This corresponds to an antenna diameter of 30 cm in the X-band. This is the largest diameter of the antenna expected to be tested in this chamber.

Since the anechoic chamber is lined with pyramidal absorbers, the diffraction from the tips of the pyramids also have to be considered. The finger pitch of the pyramids determines the scattering by them. According to Green[3] the lowest frequency at which back-scattering can occur is

$$f_{min} = c/2s$$

where s is the finger pitch and c is the velocity of light. In this chamber, $s = 7.6$ cm, and the corresponding value of f_{min} is 1.97 GHz. Hence specular reflection will occur only below this frequency.

*Present address: Atmospheric Sciences Division, Centre for Earth Science Studies, P B. 2235, Trivandrum 695 010.

This chamber is designed to have a tapered geometry due to the following reasons. Firstly, the quantity of the absorbing material needed for a tapered chamber is much less than that required for a rectangular one. Secondly, in a tapered chamber, the image sources of the transmitter will be closer to the transmitter itself, thereby minimising the wavefront distortions in the quiet zone. Again, the tapered geometry straightens out the wavefront faster than a rectangular one[4]. Tapering starts at one end of the chamber and extends till the middle. In order to avoid interference from external signals, the chamber is given a metallic shielding. Thin aluminium sheets are used for the shielding.

The anechoic chamber was constructed inside a large room of length 9.1 m and breadth 7.3 m. A portion of this rectangular room, 7.2 m × 3.6 m, was separated using wooden boards and framework for the anechoic chamber. The tapered portion begins with a slope of 25° at exactly the middle of the chamber. Aluminium sheets were nailed over the wooden framework for the shield. Over this aluminium shield, water resistant, 12-mm thick, plywood boards were fixed and the absorber was attached over these using commercial adhesives. Since the maximum reflection may occur from the centre of the back wall, this region was covered with larger pyramids. The tapered portion was covered with wedges and walkways with flat-layered absorber.

At the cubical end of the chamber there is a door to provide entry into the chamber. The tapered portion ends in another small terminal box. The interior of the portion is also covered with wedge-type absorber. The transmitting antenna is kept at the apex of the tapered portion. Fig. 1 shows a sketch of the anechoic chamber. A view of the different portions of the chamber is shown in Fig. 2.

The antenna positioner placed inside the chamber is the major instrument used in the chamber. The positioner consists of a platform which can rotate at a uniform rate of 1 rpm.

The control unit for the antenna turn-table, the transmitter, and the measuring and recording instruments are located inside the control room, adjacent to the chamber. The main features of the control panel are the following.

(i) ON/OFF switch for the motor; (ii) forward/reverse control for the turn-table;(iii) direction of rotation indicator; (iv) position indicator; (v) signal level monitor; and (vi) limit switch control.

The measuring instruments like the VSWR meter, power meter, pattern recorder, etc. are kept in the control room.

The quality of the microwave anechoic chamber depends on the reflectivity levels in the quiet zone. The

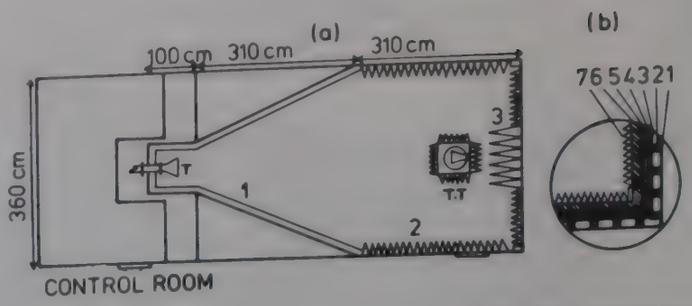

Fig. 1—(a) Construction of the anechoic chamber (T, transmitter; T.T, turn-table; 1, wedge absorber; 2, small pyramids; and 3, large pyramids); and (b) structure of the walls [1, outer plywood lining; 2, wooden structure; 3, plywood lining; 4, aluminium sheet (shield); 5, water resistant plywood lining; 6, flat absorber; and 7, pyramids]

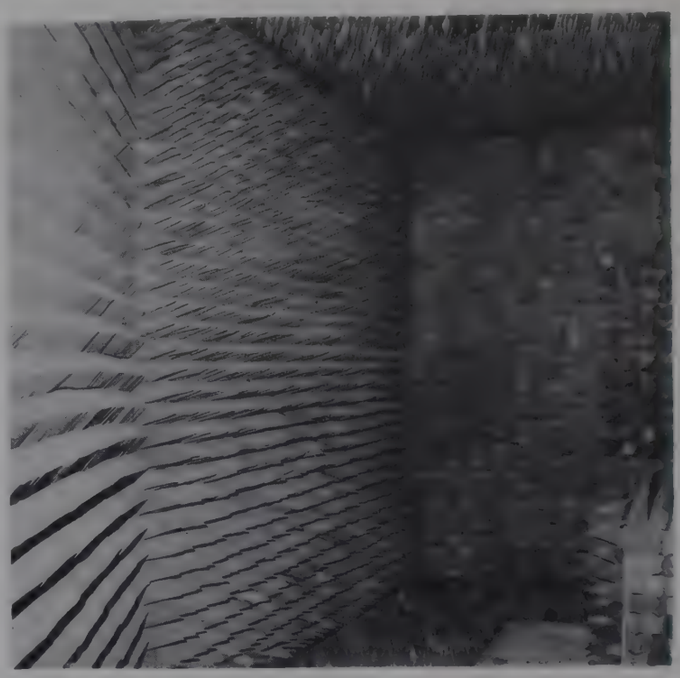

Fig. 2—Interior view of the anechoic chamber (Wedge absorbers lined in the tapered portion, pyramidal absorbers in the cubical portion and on the turn-table frame, and layered-flat absorbers paved in walkways around the turn-table can be seen.)

quiet zone is the region inside the anechoic chamber, where the total reflection from the chamber walls are below the direct radiation by the transmitting antenna by a certain specified amount.

The chamber reflectivity is defined as the average reflectivity level measured in the quiet zone. The reflectivity of the chamber was measured using the technique[5-7] of pattern comparison.

In the pattern comparison method, two identical pyramidal horns of known gain are taken. The chamber is illuminated by the transmitting antenna located along the major axis of the chamber at the tapered end. The receiving antenna is mounted on the turn-table, at the centre of the design quiet zone. The radiation pattern of the antenna is plotted and this is used as the reference pattern. The receiver is moved to a new position along the axis through a distance of 15 cm. The radiation pattern is plotted at this position. This pattern is superimposed over the reference

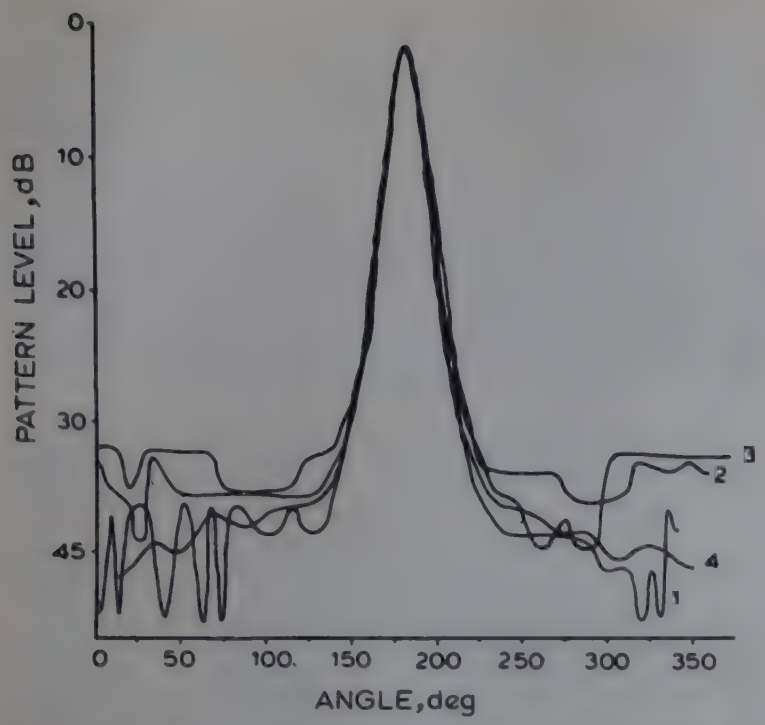

Fig. 3—Radiation patterns recorded for the pattern comparison method of evaluation (1, reference pattern; 2, 15 cm off-centre; 3, 30 cm off-centre; and 4, 45 cm off-centre)

pattern, so that the peaks coincide. This is repeated at different positions along the transverse and longitudinal directions from the centre of the quiet zone.

Fig. 3 shows some of the patterns recorded by the above method. The difference between the patterns, at specified pattern levels, say −15 dB, −20 dB, −25 dB, etc., below the mainlobe peak are noted and plotted as a function of the distance from the centre of the quiet zone. Fig. 4 shows this deviation curve. The peak-to-peak excursion of this deviation curve is noted at each pattern level. The chamber reflectivity can be then determined from standard curves supplied by Buckley[6]. The average reflectivity of this chamber determined by this method has been found to be −32 dB at X-band frequencies.

Another important chamber characteristic to be determined is the termination VSWR. The termination VSWR of anechoic chambers should be very small. Hence the conventional method of measuring the

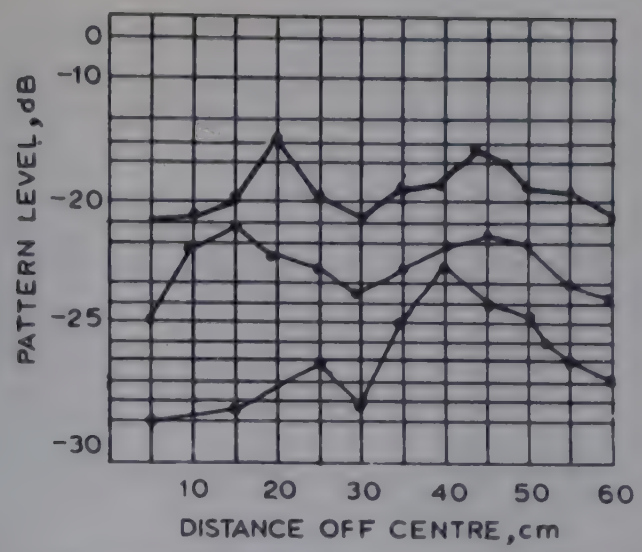

Fig. 4—Deviation at each reference-pattern level with radial distance between chamber centre and test point

VSWR with a slotted section cannot be adopted, since the mismatch introduced by the probe in the slotted section itself is of the order of the chamber mismatch. Therefore, for measuring VSWR the moving termination technique[6,8] is employed. The measured value of the termination VSWR was found to be less than 1.05.

The authors wish to acknowledge the financial assistance given by Science and Engineering Research Council, Department of Science and Technology, Government of India, New Delhi. They also thank Prof. K Sathianandan, Head of the Department of Physics, University of Cochin, for his valuable help and encouragement.

References

1 Stephen Galagan, *Microwaves (USA)*, **9** (1970) 47.
2 *Test procedure for antennas* (IEEE Press, New York), 1965.
3 Green H E, *Electr Eng Trans (Australia)*, (1977) 18.
4 Stephen Galagan, *Microwaves (USA)*, **9** (1970) 44.
5 Stephen Galagan, *Microwaves (USA)*, **9** (1970) 69.
6 Buckley E F, *Microwave J (USA)*, **6** (1963) 69.
7 Zachariah E J, *Corrugated flange technique for beam shaping of sectoral electromagnetic horn antennas*, Ph D thesis, Cochin University, Cochin, 1981.
8 Montgomery C G, *Techniques of microwave measurements* (McGraw Hill Book Company, New York), 1949.

Indian Journal of Radio & Space Physics
Vol. 13, February 1984, pp. 32-33

Phase Modulation of Microwave Signals Using Point Contact Germanium Signal Diodes

P MOHANAN & C P G VALLABHAN
Department of Physics, University of Cochin, Cochin 682 022

and

C K AANANDAN & K G NAIR
Department of Electronics, University of Cochin, Cochin 682 022

Received 4 *April* 1983

A forward-biased point contact germanium signal diode placed inside a waveguide section along the E-vector is found to introduce significant phase shift of microwave signals. The usefulness of the arrangement as a phase modulator for microwave carriers is demonstrated. While there is a less significant amplitude modulation accompanying phase modulation, the insertion losses are found to be negligible. The observations can be explained on the basis of the capacitance variation of the barrier layer with forward current in the diode.

It is well known that point contact diodes can be used as waveguide switches[1-5]. But the action of a point-contact diode in the forward-bias condition as a phase shifter of microwave signal is not mentioned in literature. In this communication, we report the properties of such a simple and effective electronic phase modulator at microwave frequencies. It essentially employs a single-point contact germanium signal diode which is placed inside a waveguide section along the E-vector. The phase modulating property is established to be primarily due to the phase-shift effect introduced by the forward-biased diode. Even though the conspicuous phase modulation is accompanied by a less significant amplitude modulation, the insertion losses are found to be extremely negligible. The use of this phenomenon for phase modulating microwave signals with different waveforms for communication purposes is demonstrated. The arrangement can also be used as a continuously variable electronic phase-shifter in UHF and microwave lines.

The phase modulator set-up consists of a single-point contact germanium signal diode (OA 79) shunted across an X-band waveguide section along the E-vector when the waveguide supports TE_{10} mode. The variations of the phase and amplitude of microwave signal with forward-bias current through the diode is monitored by a network analyser (Hewlett Packard 8410C). The effect of applying a modulating signal across the diode is also studied under both near- and far-field conditions. For far-field measurements, the modulated signal is transmitted by a pyramidal horn and received by another similar horn at a distance greater than $\frac{2D^2}{\lambda}$ where D is the maximum aperture of the horn.

The nature of the variation of phase angle with forward-bias current is shown in Fig. 1. With a single diode, the phase shift is as much as 80° for a current of 12 mA. The maximum insertion loss is found to be only less than 1 dB. VSWR measurements show that matching is improved considerably under forward bias condition. The phase shift can be increased by periodically loading the waveguide with diodes. It is

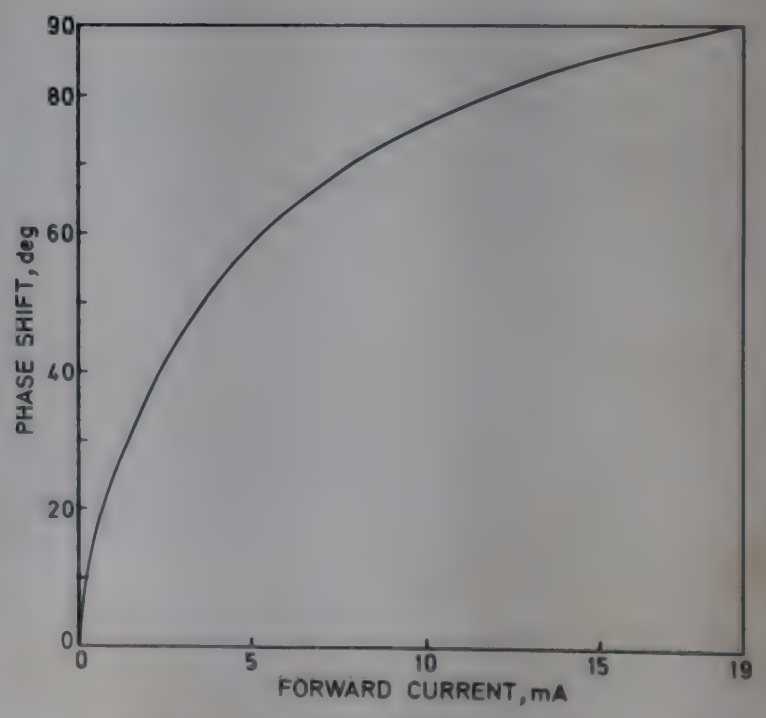

Fig. 1—Phase shift produced by the diode versus the forward current

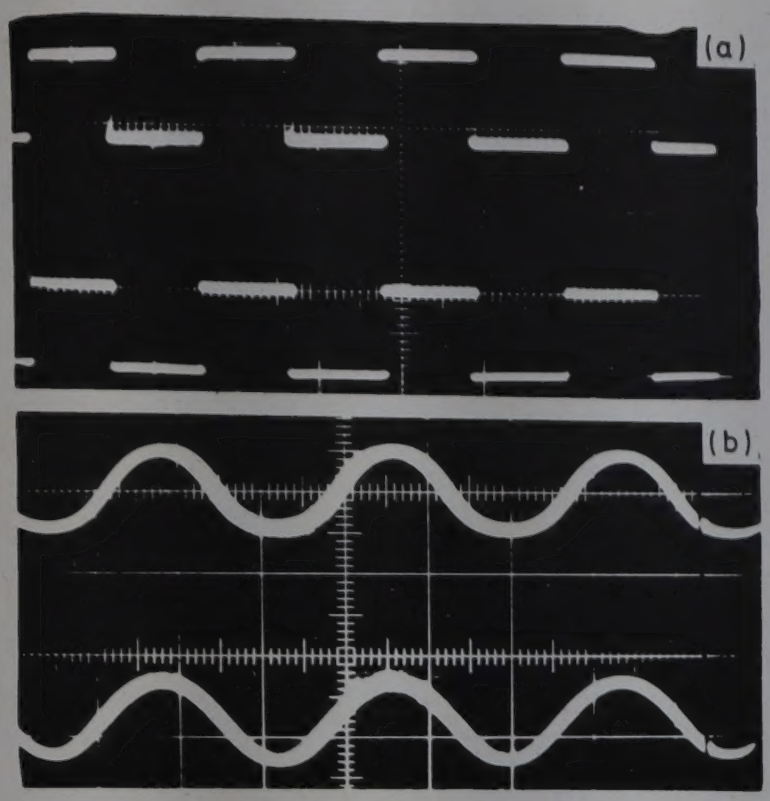

Fig. 2—Phase demodulated waveforms: (a) 10 kHz square waves; and (b) 10 kHz sine waves (Modulating signals are shown above for comparison.)

found that maximum phase shift occurs for anti-resonant spacing and minimum for resonant spacing.

In Fig. 2[(a) and (b)], photographs of phase demodulated square and sine waves of 10 kHz are presented. Due to the limitation of the bandwidth of the network analyser, modulation effects at higher frequencies could not be studied directly. It is said earlier that the phase modulation is accompanied by a small amplitude modulation which is detected by a microwave diode. Since diode is effective for amplitude modulation at video ranges, phase modulation is also expected to occur at these ranges. The maximum level required for modulating signal is of the order of 50 mV. Since the diode is active only for forward voltage, a dc bias can be applied for distortionless modulation.

An ordinary p-n junction diode can act as a phase shifter in reverse-bias condition only[6]. But a point-contact diode virtually produces no phase change in reverse-bias condition. It is found to be active as a phase shifter only when a forward voltage is given. Compared to PIN modulators, point-contact modulators are simpler, inexpensive and more readily available.

Since the capacitance of the metal semiconductor contact, which essentially forms a Schottky barrier layer, increases with the forward bias[7], the equivalent susceptance also increases with bias current, thus increasing the resultant phase variation.

In conclusion, a point-contact diode can be used as an effective, simple and low-cost phase modulator. However, its use is not restricted to microwave frequencies alone. The arrangement described here may find extensive practical uses in communication, antenna applications, electronic scanning, etc.

One of the authors (CKA) acknowledges Council of Scientific and Industrial Research, New Delhi, for providing financial assistance. The authors wish to thank Prof. K Sathianandan, Head of the Department of Physics, University of Cochin for useful discussions.

References

1 Armistead M A, Spencer E G, Hatcher R D, *Proc IRE (USA)*, **44** (1956) 1875.

2 Garver R V, Spencer E G, Harper M A, *Proc IRE Trans Microwave Theory & Tech (USA)*, **6** (1958) 378.

3 Uhler (Jr) A, *Proc IRE (USA)*, **46** (1959) 1099.

4 Garver R V, Rosado J A, Tuner E F, *IRE Trans Microwave Theory & Tech (USA)*, **8** (1960) 108.

5 Garver R V, *IEEE Trans Microwave Theory & Tech (USA)*, **13** (1965) 32.

6 Sholnik Merril I, *Radar Hand-Book*, (McGraw-Hill), 1970.

7 Yang Edward S, *Fundamentals of semiconductor devices*, (McGraw-Hill), 1978.

Papers accepted for publication

The following papers have been accepted for publication in the *Indian Journal of Radio & Space Physics.*

An Improved Empirical Model for Electron Temperature in the F2-Region: V K Pandey, K K Mahajan & V C Jain (Radio Science Division, National Physical Laboratory, New Delhi 110012).

A Semi-empirical Model of Ionospheric Electron Content at Low Latitudes for Solar Minimum: P K Bhuyan (Department of Physics, D K D College, Dergaon, Assam 785614) and Tuhi Ram Tyagi (Radio Science Division, National Physical Laboratory, New Delhi 110012).

Calculation of Spectrum & Directivity of Hard X-rays from Solar Flares: P N Khosa, R R Rausaria & Sunil Peshin (Physics Department, Regional Engineering College, Srinagar 190006) and K L Moza (Physics Department, S P College, Srinagar 190001).

Some Physical Processes in the Middle Atmosphere: B K Mukherjee, K S Raja Rao & Bh V Ramana Murty (Indian Institute of Tropical Meteorology, Pune 411005).

Accuracy of Stratospheric Wind Measurements Using Chaff Releases from RH-200 Rockets: M Devarajan, P R Parameswaran, C A Reddy & C Raghava Reddi (Space Physics Division, Vikram Sarabhai Space Centre, Trivandrum 695022).

Study of the Equatorial Ionospheric F-region Irregularities by Reflection, Backscatter & Transmission of Radiowaves: R G Rastogi (Indian Institute of Geomagnetism, Colaba, Bombay 400005).

INSTRUCTIONS TO CONTRIBUTORS

General

Contributions should reflect original work done. They should neither have been published already nor be under consideration for publication elsewhere. The manuscripts should be typewritten only on one side of good quality thesis paper, in double space and with adequate margin on all four sides of the text matter. The original and two copies thereof, all the copies complete in all respects including abstract, figures, etc., are to be submitted.

Contributions should clearly bring out the justification for undertaking the investigation and outline the exact scope of the study. Elaborate and long introductions should be avoided. Minimum essential experimental details which would enable anyone to repeat the work, should be included. Accuracy of measurements, and limitations of the results and conclusion should be clearly stated. Discussion should be limited to the strictly essential and should not repeat lengthy statements of facts/observations, which are obvious from the tabular and graphical data presented. A separate section on 'Conclusions' can be included only when they are of outstanding significance. Mere observation of trends of results should be distinguished from firm conclusions. References given at the end should be strictly limited to the essential minimum. Large-scale reproduction of all references given in another single source should be avoided unless highly relevant.

Papers must be written in clear and concise English. Good attention to spelling and grammar should be given. Long introduction should be avoided. Stanadard international nomenclature should be followed in giving names of chemical compounds. Standard abbreviations for units of measurement should be used in the text, tables and illustrations. The abbreviations should be used without fullstops.

Title—The title should be neither too brief/general nor unnecessarily long. It should reflect the content of the paper so as to derive the maximum advantage in indexing and information retrieval. A short title for use as running title should also be supplied. If a paper forms part of a series, a subtitle indicating the aspects of the work covered in the paper should be provided.

Abstract—The abstract should indicate the scope of the work and the principal findings of the paper. It should not exceed 3% of the length of the paper and, barring exceptional cases, it should not exceed 200 words. The abstract should be prepared in such a form that abstracting periodicals can use it without modification.

The abstract including the title of the paper, authors' names and affiliations, a short running title and relevant footnotes, if any, should be typed on separate sheet.

Data—Only such primary data as are essential for understanding the discussion and the main conclusions emerging from the study should be included. All such secondary data as are of interest to a specific category of readership may, if necessary, be deposited in the editorial office (or retained by the authors) for supply on demand. A footnote to this effect may be inserted at a suitable place in the paper.

Mathematical Portions—Special attention should be given to the mathematical portions of the paper. Equations must be well separated from the text and written clearly with good separation between the successive lines. The usual norms of breaking long mathematical expressions may be adhered to. Equations should be numbered consecutively in Arabic numerals with the number in parentheses near the right hand margin. Superscripts and subscripts should be clearly indicated in pencil by V and Λ signs, respectively. Capital and small letters, particularly of the same letter when both occur, as well as letters or symbols likely to be confused one for the other, should be clearly distinguished. Special characters (e.g. Greek, Script, vector, tensor, matrix, etc.) required must be indicated by marginal notes. Letters and symbols which should appear in bold face must be clearly indicated. To simplify typesetting: (i) long and complicated mathematical expressions which are frequently repeated should be replaced with single letter/symbol, without clashing with the others used in the paper; (ii) the "exp" form of complex exponential functions should be used; and (iii) to simplify fractions, the solidus (/) is to be used and fractional exponents are to be used instead of root signs, e.g.

write $\left[4\omega_{pl} K_{3\lambda}^2 \Big/ \left(\tilde{\omega} K_D^2\right)\right]^{1/2}$ and *not* $\sqrt{\dfrac{4\omega_{pl} K_{3\lambda}^2}{\tilde{\omega} K_D^2}}$

write $\exp\{-i\omega_0 (t_1 - t_2)/2\}$ and *not* $e^{-i\omega_0 (t_1 - t_2)/2}$

Tables—Tables should be typed *on separate sheets* of paper without any text matter on the page. They should be numbered consecutively in Arabic numerals and should bear brief titles. *Column headings should be brief.* Units of measurement should be abbreviated and placed below the headings. Nil results should be indicated and distinguished clearly from absence of data. Presentation of the same data both in the form of tables and graphs should be avoided. Inclusion of structural formulae inside the tables should be avoided as far as possible. Tables should be referred to in the text by numbers and not by terms like 'above', 'below', 'preceding' or 'following'.

Illustrations—All illustrations must be numbered consecutively in Arabic numerals. Captions and legends to the figures should be self-explanatory and should be typed on a separate sheet of paper and attached at the end of the manuscript. Line drawings should be made with Indian ink on white drawing paper (preferably Bristol board), cellophane sheet or tracing cloth. Histograms, probability variation curves, etc. may be prepared with hatched lines instead of thick black ink. In addition to the originals, a set of blue-prints or photostat copies should be sent. For satisfactory reproduction, the graphs and line drawings should be drawn to approximately twice the printed size.

The lettering should be uniform, preferably in stencil, so as to be *not less than 2 mm after reduction* widthwise to 3" or 6" as required. The size of geometrical shapes (used to distinguish different graphs), dots, lines, etc. should be sufficiently large to permit the necessary reduction without

loss of detail. In the case of *photographs*, prints *must be on glossy paper and contrasty*. If an illustration is taken from another publication, reference to the source should be given and prior permission secured. Illustrations should be protected by thick cardboard packing against creases, folds and broken corners during transit. Illustrations should be referred to in the text by numbers and not by terms like 'above', 'below', 'preceding' or 'following'.

Spectra, ionograms, echograms, etc. should be included only if they are essential to the discussion; otherwise only significant numerical data should be included in the text.

References—The list of references should be prepared strictly in accordance with the style followed in the journal. In the text, references to literature should be numbered consecutively, in the order of their first occurrence, and should be indicated by superscripts at the relevant places; as far as possible the placement of references on numerals or other symbols should be avoided; in such cases the reference may be given in parenthesis in running text, e.g. "this yielded for n a value of 2.3 (Ref. 5)". Full bibliographic details for all the references mentioned in the text should be listed in serial order at the end of the paper.

In citing references to research papers, names and initials of authors should be followed, in order by the title of the periodical in the abbreviated form (underlined), the volume number (two lines underneath), the year within parenthesis and the page reference [e.g. Rastogi R G, *Indian J Radio & Space Phys*, 9 (1980), 173.]. For names of periodicals, the abbreviations followed by the *Physics Abstracts* should be used. For periodicals not covered by *Physics Abstracts*, the title abbreviations should be according to the *Bibliographic Guide for Editors and Authors*, 1974, published by the American Chemical Society, Washington DC, USA; additionally the country from which the journal is published should be given in parenthesis immediately after the title abbreviation. If a paper has been accepted for publication, the names of the authors and the journal should be given followed by the words "in press" [e.g. Mitra A P, *J Atmos & Terr Phys (GB)*, 37 (1975), in press.].

In the list of references, unpublished work, accepted papers in press and personal communications should be clearly distinguished.

Even if a reference contains more than two authors, the names of all the authors with their respective initials should be given. The abbreviations *et al.*, *idem* and *ibid* should be avoided.

Reference to a book should include, in the following order: names and initials of authors, the title of the book (underlined), name of publisher and place of publication within parenthesis and year [e.g. Smylie D E, Clarke G K C & Ulrych J J, *Methods in computational physics* (Academic Press Inc., New York), 1973, 391.]. If the reference is to the work of an author published in a book by a different author or edited by a different person, the fact that it is cited from the source book should be clearly indicated [e.g. Culhane J L, cited in *Supernovae*, edited by D N Schramm (D Reidel), 1977.].

Proceedings of conferences and symposia should be treated in the same manner as books. Reference to a paper presented at a conference, the proceedings of which are not published, should include, in the following order, names and initials of authors, title of the paper (underlined), name of the conference, place where the conference was held and date (Sen A K & Trehan S K, *Field changes of the sky wave component due to a local broadcast signal during different geophysical phenomena*, Paper presented to the Symposium on Earth's Near Space Environment, National Physical Laboratory, New Delhi, 18-21 Feb. 1975).

Reference to a thesis should include the name of the author, title of the thesis (underlined), university or institution to which it was submitted and year of submission (e.g. Burg J P, *Maximum entropy spectral analysis*, Ph D thesis, Stanford University, California, 1975.).

Reference to a patent should include names of patentees, country of origin (underlined) and patent number, the organization to which the patent has been assigned within parenthesis, data of acceptance of the patent and reference to an abstracting periodical where available [Labes M M, *US Pat.* 4,066,567 (to Temple University), 3 January 1978; *Chem Abstr*, 88 (No.20)(1978), 138350 n.].

Abbreviations, symbols and units—These should conform to the style of the journal.

Frequently repeated combinations of words, e.g. sudden ionospheric disturbance (SID), point discharge current (PDC), gradual rise and fall (GRF), etc. should be abbreviated subsequently, indicating the abbreviated form in parenthesis, as shown, at the place of their first occurrence.

Nomenclature—Where too many symbols are used in the text, a section entitled 'Nomenclature', explaining the significance of the various symbols, may be given and placed just above the Acknowledgement section.

Acknowledgement—Acknowledgements should not be exuberant and must be made only to real assistance rendered in connection with the scientific work reported in the paper.

Appendixes—Appendixes, typed on separate sheets, should be numbered consecutively, in Arabic numerals, in the order of their occurrence in the text, and should be placed at the very end of the paper.

Printed and Published by Shri D.S. Sastry, Publications & Information Directorate (PID), Council of Scientific & Industrial Research, New Delhi, at PID Photocomposition-cum-Printing Unit.